Plasmon excitations and 1D - 2D dimensional crossover in quantum crossbars

I. Kuzmenko, S. Gredeskul, K. Kikoin, Y. Avishai
Department of Physics, Ben-Gurion University of the Negev, Beer-Sheva
(February 1, 2008)

Spectrum of boson fields and two-point correlators are analyzed in quantum crossbars (QCBs, a superlattice formed by m crossed interacting arrays of quantum wires), with short range inter-wire capacitive interaction. Spectral and correlation properties of double ($m = 2$) and triple ($m - 3$) QCBs are studied. It is shown that the standard bosonization procedure is valid, and the system behaves as a sliding Luttinger liquid in the infrared limit, but the high frequency spectral and correlation characteristics have either 1D or 2D nature depending on the direction of the wave vector in the 2D elementary cell of reciprocal lattice. As a result, the crossover from 1D to 2D regime may be experimentally observed. It manifests itself as appearance of additional peaks of optical absorption, non-zero transverse space correlators and periodic energy transfer between arrays ("Rabi oscillations").

I. INTRODUCTION

The behavior of electrons in arrays of $1D$ quantum wires was recognized a challenging problem soon after the consistent theory of elementary excitations and correlations in a Luttinger liquid (LL) of interacting electrons in one dimension was formulated (see[1] for a review). One of fascinating targets is a search for LL features in higher dimensions[2]. Although the Fermi liquid state seems to be rather robust for $D > 1$, the possible way to retain some $1D$ excitation modes in $2D$ and even $3D$ systems is to consider highly anisotropic objects, in which the electron motion is spatially confined in major part of the real space (e.g., it is confined to separate linear regions by potential relief). One may hope that in this case weak enough interaction does not violate the generic long-wave properties of the LL state. Arrays of interacting quantum wires may be formed in organic materials and in striped phases of doped transition metal oxides. Artificially fabricated structures with controllable configurations of arrays and variable interactions are available now due to recent achievements in nanotechnology (see, e.g., Refs. 3,4).

The simplest $2D$ ensemble of $1D$ nanoobjects is an array of parallel quantum wires. The conventional LL regime in a single $1D$ quantum wire is characterised by bosonic fields describing charge and spin modes. We confine our discussion to the charge sector (LL in the spin-gapped phase). The Hamiltonian of an isolated quantum wire may then be represented in a canonical form

$$H = \frac{\hbar v}{2} \int_{-L/2}^{L/2} dx \left\{ g\pi^2(x) + \frac{1}{g}(\partial_x \theta^2(x)) \right\}. \qquad (1)$$

Here L is the wire length, v is the Fermi velocity, θ, π are the conventional canonically conjugated boson fields and g is the dimensionless parameter which describes the strength of the interaction within the chain (see, e.g.,[1,5]). The interwire interaction may transform the LL state existing in isolated quantum wires into various phases of $2D$ quantum liquid. The most drastic transformation is caused by the *interwire* tunneling $t_\perp$ in arrays of quantum wires with *intrawire* Coulomb repulsion. This coupling constant rescales towards higher values for strong interaction ($g < 1/2$), and the electrons in array transform into $2D$ Fermi liquid[6]. The reason for this instability is the orthogonality catastrophe, i.e. the infrared divergence in the low-energy excitation spectrum that accompanies the interwire hopping processes.

Unlike interwire tunneling, the density-density or current-current interwire interactions do not modify the low-energy behavior of quantum arrays under certain conditions. In particular, it was shown recently[7–9] that an interaction of the type $W(n - n')$, which depends on the distance between the wires n and n' but does not contain current coordinates x, x', imparts the properties of a *sliding phase* to 2D array of 1D quantum wires. In this state an additional interwire coupling leaves the fixed-point action invariant under the "sliding" transformation $\theta_n \to \theta_n + \alpha_n$ and $\pi_n \to \pi_n + \alpha'_n$. The contribution of interwire coupling reduces to a renormalization of the parameters $v \to v(q_\perp)$, $g \to g(q_\perp)$ in the LL Hamiltonian (1), where $q_\perp$ is a momentum perpendicular to the chain orientation. Such LL structure can be interpreted as a quantum analog of classical sliding phases of coupled XY chains[10]. Recently, it was found[11] that a hierarchy of quantum Hall states emerges in sliding phases when a quantizing magnetic field is applied to an array.

In the present paper we concentrate on another aspect of the problem of interacting quantum wires. Instead of studying the conditions under which the LL behavior is preserved in spite of interwire interaction, we consider situations where the *dimensional crossover* from $1D$ to $2D$ occurs. Dimensional crossover is quite well studied e.g. in thin semiconducting or superconducting films where the film thickness is the control parameter that rules the crossover (see e.g. Ref. 12. It occurs in strongly anisotropic systems like quasi-one-dimensional organic conductors[13] or layered metals[14]. In the latter cases

temperature serves as a control parameter and crossover manifests itself in interlayer transport. In metals the layers appear "isolated" at high temperature, but become connected at low temperatures to manifest $3D$ conducting properties. Here we intend to study another type of dimensional crossover, i.e. a *geometrical* crossover, where the phase variable serves as a control parameter, and the excitations in quantum array demonstrate either $1D$ or $2D$ behavior in different parts of reciprocal space.

The most promising type of artificial structures where this effect is expected is a periodic $2D$ system of m crossing arrays of parallel quantum wires. We call it "quantum crossbars" (QCB). The square grids of this type consisting of 2 arrays were considered in various physical context in early papers[15–19]. In Refs. 17,18 the fragility of the LL state against interwire tunneling in the crossing areas of QCB was studied. It was found that a new periodicity imposed by the interwire hopping term results in the appearance of a low-energy cutoff $\Delta_l \sim \hbar v/a$ where a is a period of the quantum grid. Below this energy, the system is "frozen" in its lowest one-electron state. As a result, the LL state remains robust against orthogonality catastrophe, and the Fermi surface conserves its 1D character in the corresponding parts of the $2D$ Brilllouin zone (BZ). This cutoff energy tends to zero at the points where the one-electron energies for two perpendicular arrays ϵ_{k_1} and ϵ_{k_2} become degenerate. As a result, a dimensional crossover from $1D$ to $2D$ Fermi surface (or from LL to FL behavior) arises around the points $\epsilon_{F_1} = \epsilon_{F_2}$.

We study this dimensional crossover for Bose excitations (plasmons) described by canonical variables θ, π in QCB. In order to unravel the pertinent physics we consider a grid with *short-range capacitive inter-wire interaction*. This approximation seems natural for $2D$ grids of carbon nanotubes[3], or artificially fabricated bars of quantum wires with grid periods which exceed the lattice spacing of a single wire or the diameter of a nanotube. It will be shown below that this interaction can be made effectively weak. Therefore, QCB retains the $1D$ LL character for motion along the wires similarly to the case considered in Ref. 9. At the same time, the boson mode propagation along some resonant directions is also feasible. This is essentially a $2D$ process in the $2D$ BZ (or in the elementary cell of the reciprocal lattice).

We start the studies of QCB with a double QCB $m = 2$ (section II). In the first two subsections II A and II B we introduce basic notions and construct the Hamiltonian of the QCB. The main approximations are discussed in subsection II C. Here we substantiate the used method (separable interaction approximation) and show that interaction between arrays in QCB is weak. The energy spectra for square QCB and tilted QCB are described in detail in two parts II D 1 and II D 2 of subsection II D. Various correlation functions and related experimentally observable quantities (optical absorption, space correlators) are discussed in the last subsection II E. We predict here effect of peculiar "Rabi oscillations" - periodic energy transfer from one of the QCB array to another.

Triple QCB ($m = 3$) formed by three arrays lying in parallel planes are studied in Section III. Such hexagonal grids may be useful for three-terminal nanoelectronic devices[20]. The plasmon spectra of triple QCB possess some specific features in comparison with double QCB. We introduce the main notions and construct the Hamiltonian of symmetric triple QCB (subsection III A), analyse the peculiarities of the frequency spectrum (subsection III B), and illustrate them by description of triple Rabi oscillations - periodic energy transfer between all three arrays (subsection III C). The results are summarized in Conclusion. All technical details are placed in Appendices A - E.

II. DOUBLE QCB

A. Basic notions

Double QCB is a $2D$ periodic grid, which is formed by two periodically crossed arrays of $1D$ quantum wires. In experimentally realizable setups[3] these are cross-structures of suspended single-wall carbon nanotubes placed in two parallel planes separated by an inter-plane distance d. However, some generic properties of QCB may be described in assumption that QCB is a genuine $2D$ system. We assume that all wires of j-th array, $j = 1, 2$, are identical. They have the same length L_j, Fermi velocity v_j and Luttinger parameter g_j. The arrays are oriented along the unit vectors $\mathbf{e}_{1,2}$ with an angle φ between them. The periods of a crossbars along these directions are a_1 and a_2, and corresponding basic vectors are $\mathbf{a}_j = a_j \mathbf{e}_j$ (Fig.1).

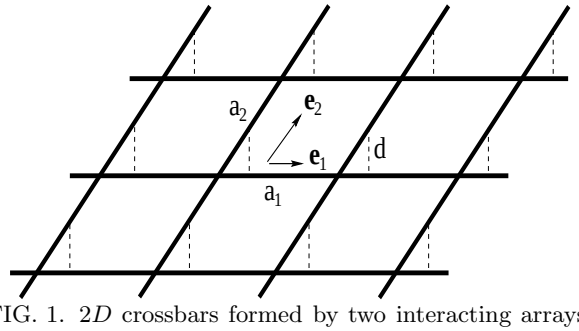

FIG. 1. $2D$ crossbars formed by two interacting arrays of parallel quantum wires. Here $\mathbf{e}_1, \mathbf{e}_2$ are the unit vectors of the superlattice, a_1, a_2 are the superlattice periods and d is the vertical interarray distance

The interaction between the excitations in different wires is assumed to be concentrated around the crossing points with coordinates $n_1\mathbf{a}_1 + n_2\mathbf{a}_2 \equiv (n_1 a_1, n_2 a_2)$.

The integers n_j enumerate the wires within the j-th array. Such interaction imposes a superperiodicity on the energy spectrum of initially one dimensional quantum wires, and the eigenstates of this superlattice are characterized by a $2D$ quasimomentum $\mathbf{q} = q_1\mathbf{g}_1 + q_2\mathbf{g}_2 \equiv (q_1, q_2)$. Here $\mathbf{g}_{1,2}$ are the unit vectors of the reciprocal superlattice satisfying the standard orthogonality relations $(\mathbf{e}_i \cdot \mathbf{g}_j) = \delta_{ij}$. The corresponding basic vectors of the reciprocal superlattice have the form $m_1Q_1\mathbf{g}_1 + m_2Q_2\mathbf{g}_2$, where $Q_j = 2\pi/a_j$ and $m_{1,2}$ are integers.

However the crossbars kinematics differs from that of a standard 2D periodic system. In conventional $2D$ systems, forbidden states in the inverse space arise due to Bragg diffraction in a $2D$ periodic potential, whereas the whole plane is allowed for wave propagation in real space, at least until the periodic potential is weak enough. A Brillouin zone is bounded by the Bragg lines. It coincides with a Wigner-Seitz cell of reciprocal lattice. In sharply anisotropic QCB most of the real space is forbidden for electron and plasmon propagation. The Bragg conditions for the wave vectors are modulated by a periodic potential unlike those in conventional $2D$ plane. These conditions are essentially one-dimensional. Corresponding BZ is not a Wigner-Seitz cell of a reciprocal lattice but the elementary cell containing a site in its center.

Indeed, the excitation motion in QCB is one-dimensional in major part of the $2D$ plane. The anisotropy in real space imposes restrictions on the possible values of $2D$ coordinates x_1, x_2 ($\mathbf{r} = x_1\mathbf{e}_1 + x_2\mathbf{e}_2$). At least one of them, e.g., x_2 (x_1) should be an integer multiple of the corresponding array period a_2 (a_1), so that the vector $\mathbf{r} = (x_1, n_2a_2)$ ($\mathbf{r} = (n_1a_1, x_2)$) characterizes the point with the $1D$ coordinate x_1 (x_2) lying at the n_2-th (n_1-th) wire of the first (second) array. As a result, one cannot resort to the standard basis of $2D$ plane waves when constructing the eigenstate with a given wave vector $\mathbf{k}$. Even in *non-interacting* arrays of quantum wires (empty superlattice) the $2D$ basis is formed as a superposition of two sets of $1D$ waves. The first of them is a set of $1D$ excitations propagating along *each* wire of the first array characterized by a unit vector $k_1\mathbf{g}_1$ with a phase shift a_2k_2 between adjacent wires. The second set is the similar manifold of excitations propagating along the wires of the second array with the wave vector $k_2\mathbf{g}_2$ and the phase shift a_1k_1. The dispersion law of these excitations has the form

$$\omega^0(\mathbf{k}) = \omega_1(k_1) + \omega_2(k_2). \tag{2}$$

The states of equal energy obtained by means of this procedure form straight lines in the $2D$ reciprocal space. For example, the Fermi surface of QCB developed from the points $\pm k_{F1,2}$ for individual quantum wire consists of two sets of lines $|k_{1,2}| = k_{F1,2}$. Respectively, the Fermi sea is not a circle with radius k_F like in the case of free $2D$ gas, but a cross in the k plane bounded by these four lines[17] (see Fig. 2). Finally, the Bragg conditions read

$$\omega_1(k_1) - omega a_1(k_1 + m_1Q_1) + \omega_2(k_2) - \omega_2(k_2 + m_2Q_2) = 0.$$

and the lines $k_1 = 0$, $|k_2| = Q_2/2$, and $|k_1| = Q_1/2$, $k_2 = 0$, satisfying these conditions, form a $2D$ BZ of double QCB.

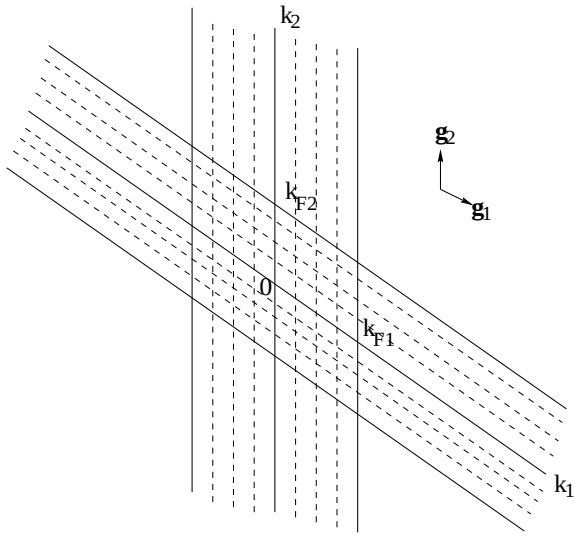

FIG. 2. Fermi surface of $2D$ metallic quantum bars in the absence of charge transfer between wires. $\mathbf{g}_1, \mathbf{g}_2$ are the unit vectors of the reciprocal superlattice

Due to the inter-wire interaction, the excitations of QCB (see Figs.3,6 below) acquire genuine two-dimensionality characterized by the quasimomentum $\mathbf{q} = (q_1, q_2)$. However, in case of weak interaction the $2D$ waves constructed from the $1D$ plane waves in accordance with the above procedure form an appropriate basis for the description of elementary excitations in QCB in close analogy with the nearly free electron approximation in conventional crystalline lattices. It is easily foreknown that a weak inter-wire interaction does not completely destroy the above quasimomentum classification of eigenstates, and the $2D$ reconstruction of the spectrum may be described in terms of wave mixing similarly to the standard Bragg diffraction in a weak periodic potential. Moreover, the classification of eigenstates of empty superlattice may be effectively used for the classification of energy bands in a real QCB superlattice where the superperiodicity is imposed by interaction.

Complete kinematics of an empty superchain (wave functions, dispersion laws, relations between quasiparticle second quantization operators) is developed in Appendix A. In terms of these $1D$ Bloch functions (see Eqs. (43), (44) of Appendix A) we construct the $2D$ basis of Bloch functions for an empty superlattice

$$\Psi_{s,s',\mathbf{q}}(\mathbf{r}) = \psi_{1,s,q_1}(x_1)\psi_{2,s',q_2}(x_2). \tag{3}$$

Here $s, s' = 1, 2, \ldots$, are the band numbers, and the $2D$ quasimomentum $\mathbf{q} = (q_1, q_2)$ belongs to the first BZ, $|q_j| \leq Q_j/2$. The corresponding eigenfrequencies are

$$\omega_{ss'}(\mathbf{q}) = \omega_{1,s}(\mathbf{q}) + \omega_{2,s'}(\mathbf{q}). \tag{4}$$

Here

$$\omega_{j,s}(\mathbf{q}) \equiv \omega_{j,s}(q_j),$$

and $\omega_{j,s}(q_j)$ is defined by Eqs. (45) below. We will use this basis in the next subsection when constructing the excitation spectrum of QCB within the reduced band scheme.

B. Hamiltonian

When turning to description of interaction in a QCB, one should refer to a real geometry of crossbars, and recollect the important fact that the equilibrium distance between two arrays is finite and large enough to supress direct electron tunneling citeRueckes. We neglect also the elastic and van der-Waals components of intertaction between real nanotubes, because these interactions are not involved in formulation of collective excitations in QCB. Then the full Hamiltonian of the QCB is

$$H = H_1 + H_2 + H_{int}, \tag{5}$$

where H_j describes the $1D$ boson field in the j-th array

$$H_1 = \frac{\hbar v_1}{2} \sum_{n_2} \int_{-L_1/2}^{L_1/2} dx_1 \Big\{ g_1 \pi_1^2 (x_1, n_2 a_2) + \frac{1}{g_1} \left(\partial_{x_1} \theta_1 (x_1, n_2 a_2)\right)^2 \Big\},$$

$$H_2 = \frac{\hbar v_2}{2} \sum_{n_1} \int_{-L_2/2}^{L_2/2} dx_2 \Big\{ g_2 \pi_2^2 (n_1 a_1, x_2) + \frac{1}{g_2} \left(\partial_{x_2} \theta_2 (n_1 a_1, x_2)\right)^2 \Big\},$$

and θ_j, π_j are the conventional canonically conjugated boson fields (see, e.g., Ref. 5).

The interwire interaction results from a short–range contact capacitive coupling in the crosses of bars,

$$H_{int} = \sum_{n_1, n_2} \int dx_1 dx_2 V(x_1 - n_1 a_1, n_2 a_2 - x_2) \times \rho_1(x_1, n_2 a_2) \rho_2(n_1 a_1, x_2),$$

where the integration is restricted by the area $-L_j/2 \leq x_j \leq L_j/2$. Here $\rho_i(\mathbf{r})$ are density operators, and $V(\mathbf{r}_1 - \mathbf{r}_2)$ is a short-range interwire interaction. Physically, it represents the Coulomb interaction between charge fluctuations

$$e\zeta\left(\frac{x_j - n_j a_j}{r_j}\right), \quad \zeta(\xi) = \zeta(-\xi), \quad \zeta(0) = 1, \tag{6}$$

around the crossing point $(n_1 a_1, n_2 a_2)$. The size of the fluctuation on the wire of the j-th array, is determined by the screening radius r_j within the wire. One may neglect the inter-wire tunneling and restrict oneself by the capacitive interaction only, provided the vertical distance between the wires d is substantially larger than the screening radiuses r_j. Therefore the interaction has the form,

$$V(\mathbf{r}) = \frac{V_0}{2} \Phi\left(\frac{x_1}{r_1}, \frac{x_2}{r_2}\right),$$

where the function $\Phi(\xi_1, \xi_2)$ is

$$\Phi(\xi_1, \xi_2) = \frac{\zeta_1(\xi_1)\zeta_2(\xi_2)}{\sqrt{1 + \frac{|\mathbf{r}_{12}|^2}{d^2}}}, \tag{7}$$

$$\mathbf{r}_{12} = r_1 \xi_1 \mathbf{e}_1 - r_2 \xi_2 \mathbf{e}_2.$$

It is seen from these equations that $\Phi(\xi_1, \xi_2)$ vanishes for $|\xi_{1,2}| \geq 1$ and is normalized by condition $\Phi(0, 0) = 1$. The effective coupling strength is

$$V_0 = \frac{2e^2}{d}. \tag{8}$$

In terms of boson field operators θ_i, the interaction is written as

$$H_{int} = V_0 \sum_{n_1, n_2} \int dx_1 dx_2 \Phi\left(\frac{x_1 - n_1 a_1}{r_1}, \frac{n_2 a_2 - x_2}{r_2}\right) \times \partial_{x_1} \theta_1(x_1, n_2 a_2) \partial_{x_2} \theta_2(n_1 a_1, x_2).$$

In the quasimomentum representation (3) the full Hamiltonian (5) acquires the form,

$$H = \frac{\hbar v g}{2} \sum_{j=1}^{2} \sum_{s, \mathbf{q}} \pi^\dagger_{js\mathbf{q}} \pi_{js\mathbf{q}} + \frac{\hbar}{2vg} \sum_{jj'=1}^{2} \sum_{s, s', \mathbf{q}} W_{jsj's'\mathbf{q}} \theta^\dagger_{js\mathbf{q}} \theta_{j's'\mathbf{q}}, \tag{9}$$

where $\sqrt{vg/v_j g_j}\theta_{js\mathbf{q}}$ and $\sqrt{v_j g_j/vg}\pi_{js\mathbf{q}}$ are the Fourier components of the boson fields θ_j and π_j, and effective velocity and coupling are $v = \sqrt{v_1 v_2}$, $g = \sqrt{g_1 g_2}$ respectively.

The matrix elements for interwire coupling are given by:

$$W_{jsj's'\mathbf{q}} = \omega_{js}(q_j)\omega_{j's'}(q_{j'})\left[\delta_{jj'}\delta_{ss'} + \phi_{jsj's'\mathbf{q}}\left(1-\delta_{jj'}\right)\right].$$

Here

$$\omega_{js}(q_j) = v_j\left(\left[\frac{s}{2}\right]Q_j + (-1)^{s-1}|q_j|\right), \tag{10}$$

are eigenfrequencies of the "unperturbed" $1D$ mode (see Eq. (45) of Appendix A), pertaining to an array j, band s and quasimomentum $\mathbf{q} = q_j\mathbf{g}_j$. The coefficients

$$\phi_{1s2s'\mathbf{q}} = \phi(-1)^{s+s'}\mathrm{sign}(q_1q_2)\Phi_{1s2s'\mathbf{q}},$$
$$\phi = \frac{gV_0r_0^2}{\hbar va}, \quad r_0 = \sqrt{r_1r_2}, \quad a = \sqrt{a_1a_2},$$

are proportional to the dimensionless Fourier component of the interaction strengths

$$\Phi_{1s2s'\mathbf{q}} = \int d\xi_1 d\xi_2 \Phi(\xi_1,\xi_2)e^{-i(r_1q_1\xi_1 + r_2q_2\xi_2)} \times u^*_{1,s,q_1}(r_1\xi_1)u^*_{2,s',q_2}(r_2\xi_2) = \Phi^*_{2s'1s\mathbf{q}}.$$

The Hamiltonian (9) describes a system of coupled harmonic oscillators, which can be *exactly* diagonalized with the help of a certain canonical linear transformation (note that it is already diagonal with respect to the quasimomentum $\mathbf{q}$). The diagonalization procedure is, nevertheless, rather cumbersome due to the mixing of states belonging to different bands and arrays. However, it will be shown below that provided $d \gg r_{1,2}$, a separable potential approximation is applicable, that shortens calculations noticeably.

C. Approximations

As it was already mentioned, we consider the rarefied QCB with short range capacitive interaction. In the case of QCB formed by nanotubes, this is a Coulomb interaction screened at a distance of the order of the nanotube radius[21] R_0, therefore $r_0 \sim R_0$. The minimal radius of a single-wall carbon nanotube is about $R_0 = 0.35 \div 0.4nm$ (see Ref. 22). The intertube vertical distance d in artificially produced nanotube networks is estimated as $d \approx 2$nm (see Ref. 3) Therefore the ratio $r_0^2/d^2 \approx 0.04$ is really small and *the dimensionless interaction* $\Phi(\xi_1,\xi_2)$ (7) *in the main approximation is separable*

$$\Phi(\xi_1,\xi_2) \approx \Phi_0(\xi_1,\xi_2) = \zeta_1(\xi_1)\zeta_2(\xi_2). \tag{11}$$

It should be noted that the interaction in this form is an even function of its arguments, and the odd correction to the Φ_0 is of order r_0^2/d^2, whereas Φ_0 is of order of 1.

To diagonalize the Hamiltonian (9), one should solve the system of equations of motion for the field operators. Generalized coordinates θ satisfy the equations

$$\left[\omega_{1s}^2(q_1) - \omega^2\right]\theta_{1s\mathbf{q}} + \sqrt{\varepsilon}\phi_{1s}(q_1)\omega_{1s}(q_1) \times\frac{r_0}{a}\sum_{s'}\phi_{2s'}(q_2)\omega_{2s'}(q_2)\theta_{2s'\mathbf{q}} = 0, \quad s = 1,2,\ldots, \tag{12}$$

and the similar equations obtained by permutation $1 \leftrightarrow 2$. Here

$$\phi_{js}(q) = (-1)^s\mathrm{sign}(q)\int d\xi\zeta_j(\xi)e^{ir_0q\xi}u_{jsq}(r_0\xi), \tag{13}$$

Bloch amplitudes $u_{jsq}(r_0\xi)$ are defined by Eqs. (44) of Appendix A, and

$$\varepsilon = \left(\phi\frac{a}{r_0}\right)^2 = \left(\frac{gV_0r_0}{\hbar v}\right)^2. \tag{14}$$

Due to separability of the interaction, equations of motion (12) can be solved exactly. Corresponding square eigenfrequencies are determined by the characteristic equation

$$F_{1q_1}(\omega^2)F_{2q_2}(\omega^2) = \frac{1}{\varepsilon}, \tag{15}$$

where

$$F_{jq}(\omega^2) = \frac{r_j}{a_j}\sum_s\frac{\phi_{js}^2(q)\omega_{js}^2(q)}{\omega_{js}^2(q)-\omega^2}. \tag{16}$$

The function $F_{jq}(\omega^2)$ has a set of poles at $\omega^2 = \omega_{js}^2(q)$, $s = 1,2,3,\ldots$. For squared frequency smaller than all squared initial eigenfrequencies $\omega_{js}^2(q)$, i.e. within the interval $[0,\omega_{j1}^2]$, this is a positive and growing function. Its minimal value F_j on the interval is reached at $\omega^2 = 0$, and it does not depend on quasimomentum q

$$F_{jq}(0) = \frac{r_j}{a_j}\sum_s\phi_{js}^2(q) = \int d\xi\zeta_j^2(\xi) \equiv F_j \tag{17}$$

(here Eqs. (16) and (13) are used). If parameter ε is smaller than its critical value

$$\varepsilon_c = \frac{1}{F_1F_2}, \tag{18}$$

then all solutions ω^2 of the characteristic equation are positive. When ε increases, the lowest QCB mode softens and its square frequency vanishes *in a whole BZ* at $\varepsilon = \varepsilon_c$. For exponential charge density distribution $\zeta(\xi) = \exp(-|\xi|)$, one obtaines $\varepsilon_c \approx 1$.

In our model the dimensionless interaction ε in Eq.(14) can be written as

$$\varepsilon = \left(\frac{2R_0}{d}\frac{ge^2}{\hbar v}\right)^2. \tag{19}$$

For nanotube QCB, the first factor within parentheses is about 0.35. The second one which is nothing but the

corresponding QCB "fine structure" constant, can be estimated as 0.9 (we used the values of $g = 1/3$ and $v = 8 \times 10^7$cm/sec, see Ref. 23). Therefore ε approximately equals 0.1, so this parameter is really small. Thus the considered system is stable, its spectrum is described by Eqs.(15), (16) with a *small* parameter ε.

The general Eq.(15) reduces in infrared limit $\mathbf{q}, \omega \to 0$ to an equation describing the spectrum of two coupled sliding phases. i.e. $1:1$ arrays in accordance with classification , offered in Ref. 9. Equation (3.13) of this paper is a long wave limit of our equation (47) derived in Appendix B. Therefore the general analysis of stability of the LL fixed point is appicable in our approach.

D. Spectrum

Due to the smallness of interaction, the systematics of unperturbed levels and states is grossly conserved, at least in the low energy region corresponding to the first few energy bands. This means that perturbed eigenstates could be described by the same quantum numbers (array number, band number and quasimomentum) as the unperturbed ones. Such a description fails in two specific regions of reciprocal space. The first of them is the vicinity of lines $q_j = nQ_j/2$ with n integer. Indeed, as it follows from the equations of motion (12), around these lines the interband mixing is significant. These lines with $n = \pm 1$ include BZ boundaries. Because of this BZ which is, generally speaking, non relevant, and in this subsection we refer mostly to BZ.

The second region is the vicinity of the lines where the resonance conditions are fulfilled

$$\omega_{1s}^2(q_1) = \omega_{2s'}^2(q_2). \tag{20}$$

Here inter-array mixing within the same energy band ($s = s'$) or between neighboring bands ($s \neq s'$) is significant. In what follows we will pay attention first of all to these two regions because in the rest of the BZ the initial systematics of the energy spectrum can be successfully used.

Equations (12), (15), describing the wave functions and the dispersion laws are analysed in Appendix B. We describe below some of these dispersion qurves for two types of QCB basing on this analysis.

1. Square QCB

We start with the simplest case of square QCB formed by identical wires. This means that all parameters (wire length, space period, Fermi velocity, LL parameter, screening radius) are the same for both arrays. The corresponding BZ and is also a square (see Fig.3). Resonant lines are the diagonals of BZ.

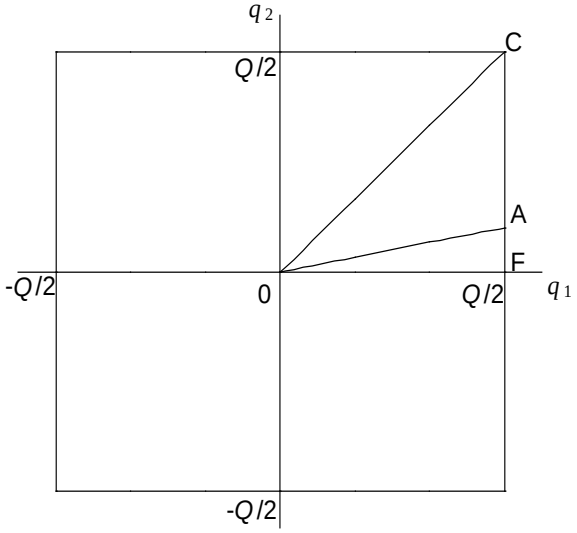

FIG. 3. Two dimensional BZ of square QCB.

In the major part of the BZ, for quasimomenta $\mathbf{q}$ lying far from the diagonals, each eigenstate mostly conserves its initial systematics, i.e. belongs to a given array, and mostly depends on a given quasimomentum component. Corresponding dispersion laws remain linear being slightly modified near the BZ boundaries only. The main change is therefore the renormalization of the plasmon velocity.

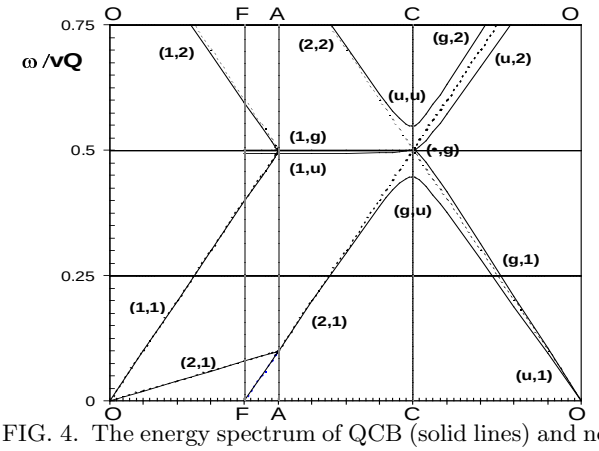

FIG. 4. The energy spectrum of QCB (solid lines) and noninteracting arrays (dashed lines) for quasimomenta at the lines OA, FC, and OC of BZ

In the left part of Fig.4 we displayed dispersion curves corresponding to quasimomenta belonging to a generic OA line in BZ. In what follows we use (j, s) notations for the unperturbed boson propagating along the j-th array in the s-th band. Then the lowest curve in this part of Fig.4 is, in fact, the slightly renormalized dispersion of a $(2, 1)$ boson. The middle curve describes $(1, 1)$ boson,

and the upper curve is the dispersion of a $(1,2)$ boson. The fourth frequency corresponding to a $(2,2)$ boson, is far above and is not displayed in the figure. It is seen that the dispersion remains linear along the whole line OA except a nearest vicinity of the BZ boundary (point A in Fig.3).

Dispersion curves corresponding to quasi momenta lying at the BZ boundary $q_1 = Q/2$, $0 \le q_2 \le Q/2$ (line FC in Fig.3) are displayed in the central part in Fig.4). The characteristic feature of this boundary is the intraband degeneracy in one of two arrays. Indeed, in zero approximation, two modes $(1,s)$, $s = 1,2$, propagating along the first array are degenerate with unperturbed frequency $\omega = 0.5$. The interaction lifts the degeneracy. This interaction occurs to be repulsive at the BZ boundaries. As a result the lowest of two middle curves in Fig.4 corresponds to $(1,u)$ boson, and upper of them describes $(1,g)$ boson. Here the indices g,u denote a boson parity with respect to the transposition of the band numbers. Note that $(1,g)$ boson exactly conserves its unperturbed frequency $\omega = 0.5$. The latter fact is related to the square symmetry of the QCB.

Two others curves correspond to almost non pertubed bosons of the second array. The lowest curve describes the dispersion of the $(2,1)$ wave. Its counterpart in the second band $(2,2)$ is described by the highest curve in the figure. Their dispersion laws are nearly linear, and deviations from linearity are observed only near the corner of the BZ (point C in Fig.3).

Consider now dispersion relations of modes with quasi–momenta on the diagonal OC of BZ and start with $\mathbf{q}$ not too close to the BZ corner C ($q_1 = q_2 = Q/2$). This diagonal is actually one of the resonance lines. Two modes in the first band coressponding to different arrays are strongly mixed. They mostly have a definite j-parity with respect to transposition of array numbers $j = 1,2$. Interaction between these modes occurs to be attractive (repulsive) for $q_1 q_2 > 0$ ($q_1 q_2 < 0$). Therefore the odd modes (u,s), at the BZ diagonal OC $s = 1,2$, correspond to lower frequencies and the even modes (g,s) correspond to higher ones. The corresponding dispersion curves are displayed in the right part of Fig.4.

At the BZ corner $q_1 = q_2 = Q/2$ (point C in Fig.3) all four initial modes $j,s = 1,2$ are degenerate in the lowest approximation. This four-fold degeneracy results from the square symmetry of BZ (the resonant lines are diagonals of the Z). Weak inter-wire interaction partially lifts the degeneracy, however the split modes have a definite s-parity with respect to transposition of band numbers $s = 1,2$. The lowest frequency corresponds mostly to (g,u) boson, symmetric with respect to transposition of array numbers, but antisymmetric with respect to the transposition of band numbers. The upper curve describes a (u,u) boson with odd both j-parity and s-parity. The two middle modes with even band parity, (g,g) and (u,g) bosons, remain degenerate and their frequencies conserve the unperturbed value $\omega = 0.5$. This also results from the square symmetry of QCB (7).

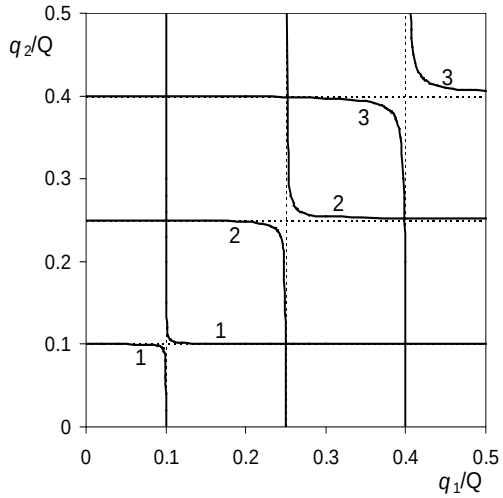

FIG. 5. Lines of equal frequency of the lowest mode for QCB (solid lines) and for noninteracting arrays (dashed lines). The lines $1,2,3$ correspond to the frequencies $\omega_1 = 0.1$, $\omega_2 = 0.25$, $\omega_3 = 0.4$

All these results show that the quantum states of the $2D$ QCB conserve the quasi $1D$ character of the Luttinger–like liquid in major part of momentum space, and that $2D$ effects can be successfully calculated within the framework of perturbation theory. However, bosons with quasimomenta close to the resonant line (diagonal OC) of the BZ are strongly mixed bare $1D$ bosons. These excitations are essentially two-dimensional, and therefore the lines of equal energy in this part of the BZ are modified by the $2D$ interaction (see Fig.5). It is clearly seen that deviations from linearity occur only in a small part of the BZ. The crossover from LL to FL behavior around isolated points of the BZ due to a single-particle hybridization (tunneling) for Fermi excitations was noticed in Refs. 17,18, where a mesh of horizontal and vertical stripes in superconducting cuprates was studied.

2. Tilted QCB

Now we consider the spectrum of a generic double QCB. In this case all parameters (wire length, space period, Fermi velocity, LL parameter, screening radius) depend, generally speaking, on the array index j. In what follows we refer to such a QCB as a tilted QCB. Now the resonance condition (20) is fulfilled not at the BZ diagonal but at the resonant polygonal line. Its part ODE, lying in the first quarter of the BZ, is displayed in Fig.6 (all figures of this subsection correspond to specific values $v_2 Q_2 = 1, \quad v_1 Q_1 = 1.4$).This results in qualitative

changes of the spectrum that are related first of all to the appearance of two points D and E of the three-fold degeneracy for a titled QCB (Fig.6) instead of a single point C of four-fold degeneracy for a square QCB (Fig.3).

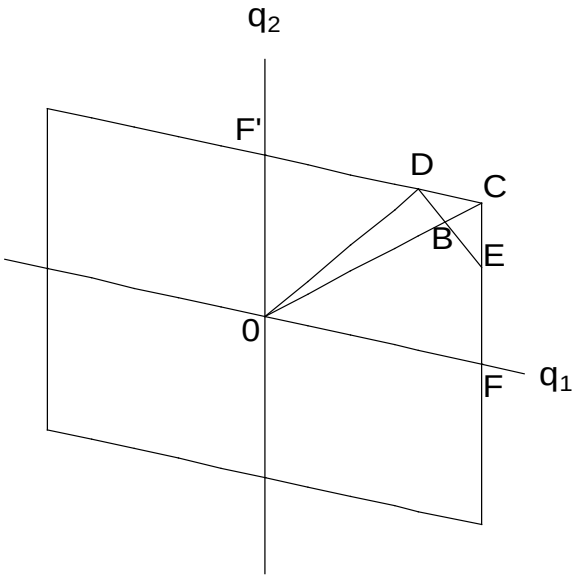

FIG. 6. BZ of a titled QCB

We start with the resonant line ODE (Fig.7). The dispersion curves at its OD part and the symmetry properties of the corresponding eigenstates are similar to those at the OC resonant line for the square QCB (Fig.3). The only difference is that instead of the four-fold degeneracy at the BZ corner C of the square QCB, there is a three-fold degeneracy at the point D lying at the BZ boundary. A completely new situation takes place at the DE line, where two other modes $(1,1)$ and $(2,2)$, corresponding to different arrays and different bands, are degenerate. The interaction lifts this degeneracy and the two middle lines in Fig.7 describe even (g) and odd (u) combinations of these modes. The even mode corresponds to the lowest frequency and the odd mode corresponds to the higher one. At the point E one meets another type of a three-fold degeneracy described in more detail in the next paragraph..

Dispersion curves corresponding to quasi momenta lying at the BZ boundary $q_1 = Q_1/2$, $0 \le q_2 \le Q_2/2$ (FC line in Fig.6) and $q_2 = Q_2/2$, $0 \le q_1 \le Q_1/2$ (CF' line in Fig.6), are displayed in Fig.8. The lowest and the highest curves in the FE part of the latter figure, describe two waves propagating along the second array. They are nearly linear, and deviations from linearity are observed only near the point E where the interaction has a resonant character. Two modes propagating along the first array, in zero approximation, are degenerate with an unperturbed frequency $\omega = 0.7$. The interaction lifts the degeneracy. The lowest of the two middle curves corresponds to $(1,u)$ boson, and the upper of one describes $(1,g)$ boson. Note that $(1,g)$ boson conserves its unperturbed frequency $\omega = 0.7$. The latter fact is related to the symmetry $\zeta_j(\xi) = \zeta_j(-\xi)$ of the separable interaction (6). At the point E, the two modes propagating along the first array and the mode propagating along the second array in the second band are degenerate. Interactions lifts the degeneracy, and, as a result, the $(1,u)$ and $(2,2)$ waves are strongly mixed and the eigenmodes are their even (highest frequency) and odd (lowest frequency) combinations, and the $(1,g)$ mode (middle level).

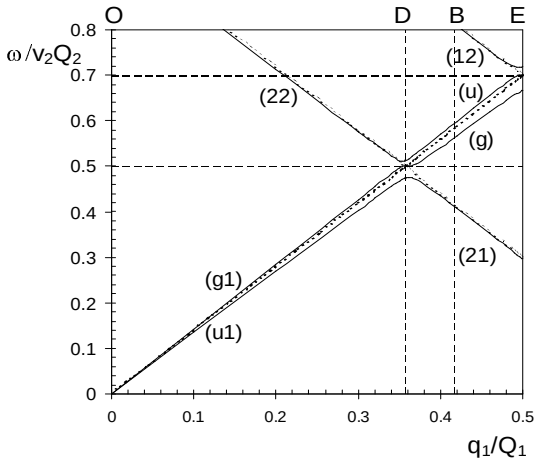

FIG. 7. The energy spectrum of a tilted QCB (solid lines) and noninteracting arrays (dashed lines) for quasimomenta on the resonant line of the BZ (line ODE in Fig.6)

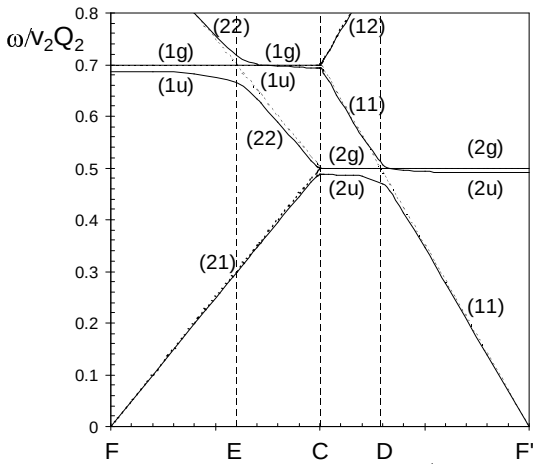

FIG. 8. Energy spectrum of a tilted QCB (solid lines) and noninteracting arrays (dashed lines) for quasimomenta at the BZ boundary (line FCF' in the Fig.6)

There are two separate degeneracies within each array at the corner C of a titled QCB BZ. Both of them are related to interband mixing conserving array index. The spectral behavior along the CF' boundary of the BZ is similar to that considered above but in the vicinity of the point D of three-fold degeneracy. Here, two modes propagating along the second array in the separable potential

approximation (11) remain degenerate. This degeneracy is lifted only if deviation from separability is accounted for.

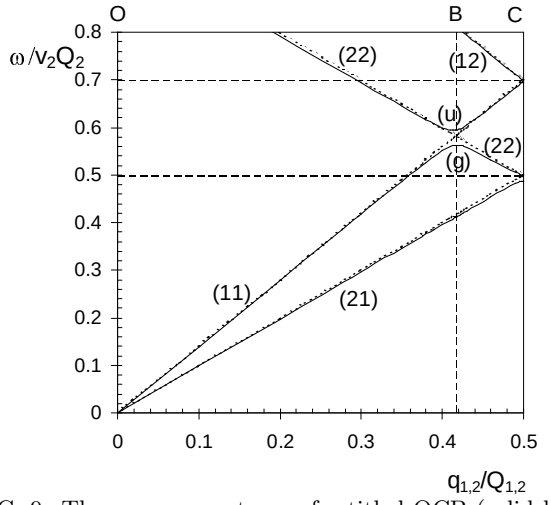

FIG. 9. The energy spectrum of a titled QCB (solid lines) and noninteracting arrays (dashed lines) for quasimomenta on the BZ diagonal (line OC in Fig.6)

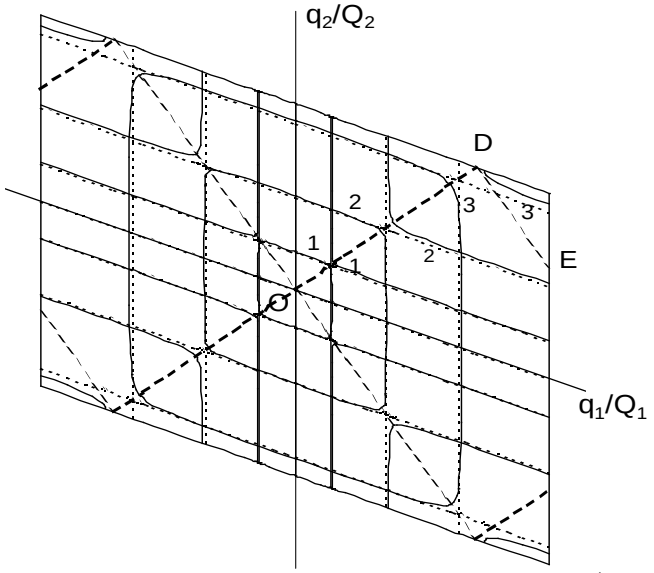

FIG. 10. Lines of equal frequency for a tilted QCB (solid lines) and noninteracting arrays (dashed lines). Lines $1, 2, 3$ correspond to frequencies $\omega_1 = 0.1$, $\omega_2 = 0.25$, $\omega_3 = 0.45$.

The diagonal OC of a tilted QCB BZ represents a new type of generic line, that crosses a resonant line (Fig.9). Here the spectrum mostly conserves its initial systematics, i.e. belongs to a given array, and mostly depends on a given quasimomentum component. However, at the crossing point B, the modes $(1, 1)$ and $(2, 2)$, corresponding to both different arrays and bands, become degenerate (two middle dashed lines in Fig.9). Interaction between the wires lifts the degeneracy. The eigenstates of QCB have a definite parity with respect to transposition of these two modes. The lowest and upper of two middle lines corresponds to even (g) and odd (u) mode, respectively.

Like in square QCB, bosons with quasimomenta close to the resonant lines are strongly mixed bare $1D$ bosons. These excitations are essentially two-dimensional, and therefore lines of equal energy in the vicinity of the resonant lines are modified by the $2D$ interaction (see Figs.10,11). Deviations from $1D$ behaviour occur only in this small part of the BZ. For $\omega < 0.5v_2Q_2$ the lines of equal energy within BZ consist of closed line around the BZ center and four open lines (within the extendend bands scheme these lines are certainly closed) around the BZ corners (lines 1, 2, 3 in Fig.10). At the line OD in BZ, the modes of QCB are strongly coupled bare bosons propagating along both arrays in the first band.

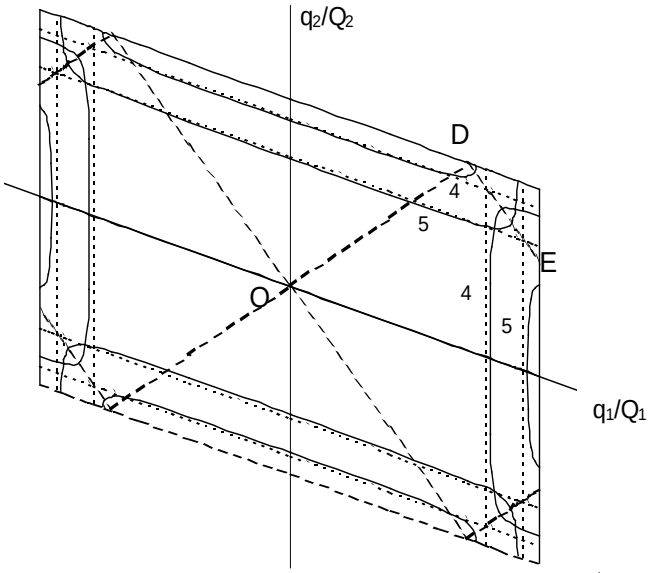

FIG. 11. Lines of equal frequency for a tilted QCB (solid lines) and noninteracting arrays (dashed lines). Lines $4, 5$ in the lower panel correspond to frequencies $\omega_4 = 0.55$, $\omega_5 = 0.65$

For $0.5v_2Q_2 < \omega < 0.5v_1Q_1$ (lines 4, 5 in Fig.11) the topology of lines of equal energy is modified. In this case lines of equal energy within the BZ consist of four open lines. The splitting of lines at the direction DE corresponds to strong coupling of modes propagating along the first array in the first band with those propagating along the second array in the second band.

E. Correlations and Observables

The structure of the energy spectrum analyzed above predetermines optical and transport properties of QCB.

We consider here three types of correlation functions manifesting dimensional crossover in QCB.

1. Optical Absorption

We start with *ac* conductivity

$$\sigma_{jj'}(\mathbf{q},\omega) = \sigma'_{jj'}(\mathbf{q},\omega) + i\sigma''_{jj'}(\mathbf{q},\omega). \quad (21)$$

The real part $\sigma'_{jj'}(\mathbf{q},\omega)$ determines an optical absorption. The spectral properties of *ac* conductivity are given by a current–current correlator

$$\sigma_{jj'}(\mathbf{q},\omega) = \frac{1}{\omega}\int_0^\infty dt e^{i\omega t}\left\langle\left[J_{j1\mathbf{q}}(t), J^\dagger_{j'1\mathbf{q}}(0)\right]\right\rangle. \quad (22)$$

Here $J_{js\mathbf{q}} = \sqrt{2}vg\pi_{js\mathbf{q}}$ is a current operator for the j-th array (we restrict ourselves to the first band, for the sake of simplicity).

The current-current correlator for non-interacting wires is reduced to the conventional LL expression[1],

$$\left\langle\left[J_{j1\mathbf{q}}(t), J^\dagger_{j'1\mathbf{q}}(0)\right]\right\rangle_0 = -2ivg\omega_{j1\mathbf{q}}\sin(\omega_{j1\mathbf{q}}t)\delta_{jj'}$$

with metallic-like peak

$$\sigma'_{jj'}(\mathbf{q},\omega>0) = \pi vg\delta(\omega-\omega_{j1\mathbf{q}})\delta_{jj'}. \quad (23)$$

For QCB this correlator is calculated in Appendix C. Its analysis leads to the following results.

The longitudinal absorption

$$\sigma'_{11}(\mathbf{q},\omega) \propto (1-\phi^2_{1\mathbf{q}})\delta(\omega-\tilde\omega_{1\mathbf{q}}) + \phi^2_{1\mathbf{q}}\delta(\omega-\tilde\omega_{2\mathbf{q}}) \quad (24)$$

contains well pronounced peak on the modified first array frequency and weak peak at the second array frequency (the parameter $\phi_{1\mathbf{q}}$, defined by Eq. (58)of Appendix B, is small). The modified frequencies $\tilde\omega_{1\mathbf{q}}$ and $\tilde\omega_{2\mathbf{q}}$ coincide with the eigenfrequencies $\omega_{+1\mathbf{q}}$ and $\omega_{-2\mathbf{q}}$ respectively, if $\omega_{1\mathbf{q}} > \omega_{2\mathbf{q}}$. In the opposite case the signs $+,-$ should be changede to the opposite ones.

The transverse absorption component contains two weak peaks

$$\sigma'_{12}(\mathbf{q},\omega) \propto \phi_{1\mathbf{q}}\left[\delta(\omega-\tilde\omega_{1\mathbf{q}}) + \delta(\omega-\tilde\omega_{2\mathbf{q}})\right]. \quad (25)$$

At the resonant line, the results change drastically. Both longitudinal and transverse components of the optical absorption contain two well pronounced peaks corresponding to slightly split modified frequencies

$$\sigma'_{11}(\mathbf{q},\omega) \propto \frac{1}{2}\left[\delta(\omega-\tilde\omega_{1\mathbf{q}}) + \delta(\omega-\tilde\omega_{2\mathbf{q}})\right]. \quad (26)$$

2. Space Perturbation

One of the main effects specific for QCB is the appearance of non-zero transverse momentum–momentum correlation function. In space-time coordinates $(\mathbf{x},t)$ its representation reads,

$$G_{12}(\mathbf{x},t) = i\left\langle[\pi_1(x_1,0;t), \pi_2(0,x_2;0)]\right\rangle. \quad (27)$$

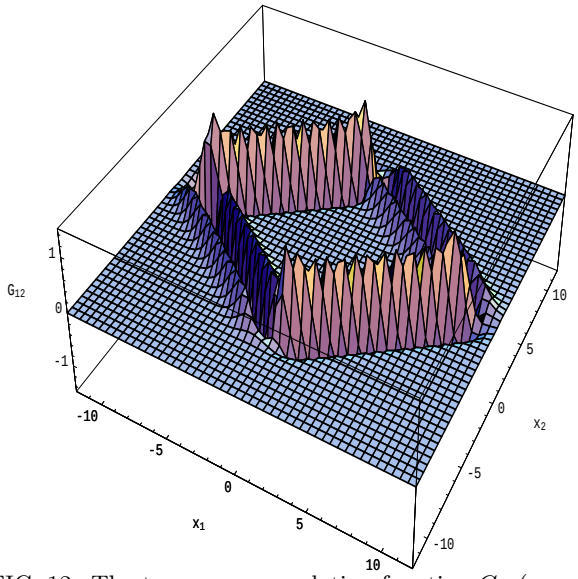

FIG. 12. The transverse correlation function $G_{12}(x_1,x_2;t)$ for $r_0 = 1$ and $vt = 10$

This function describes the momentum response at the point $(0,x_2)$ of the second array for time t caused by an initial ($t=0$) perturbation localized in coordinate space at the point $(x_1,0)$ of the first array. Standard calculations similar to those described above, lead to the following expression,

$$G_{12}(\mathbf{x};t) = \frac{V_0 r_0^2}{4\pi^2\hbar}\int_{-\infty}^{\infty} dk_1 dk_2 \phi_1(k_1)\phi_2(k_2)k_1k_2$$
$$\times \sin(k_1x_1)\sin(k_2x_2)\frac{v_2k_2\sin(v_2k_2t) - v_1k_1\sin(v_1k_1t)}{v_2^2k_2^2 - v_1^2k_1^2},$$

where $\phi_j(k)$ is the form-factor (13) written in the extended BZ. This correlator is shown in Fig.12. It is mostly localized at the line determined by the obvious kinematic condition

$$\frac{|x_1|}{v_1} + \frac{|x_2|}{v_2} = t.$$

The time t in the r.h.s. is thea total time of plasmon propagation from the starting point $(x_1,0)$ to the final point $(0,x_2)$ or vice versa, along any of the shortest ways compatible with a restricted geometry of the $2D$ grid. The finiteness of the interaction radius slightly spreads this peak and modifies its profile.

Further manifestation of the 2D character of QCB system is related to the possibility of periodic energy transfer between the two arrays. Consider an initial perturbation which excites a plane wave with amplitude θ_0 within the first array in the system of *non*-interacting arrays,

$$\theta_1(x_1, n_2a_2; t) = \theta_0 \sin(q_1x_1 + q_2n_2a_2 - v_1|q_1|t).$$

If the wave vector $\mathbf{q}$, satisfying the condition $|\mathbf{q}| << Q_{1,2}/2$, is not close to the resonant line of the BZ, weak interarray interaction $\phi = \varepsilon r_0/a$ slightly changes the θ_1 component and leads to the appearance of a small $\theta_2 \sim \phi$ component. But for $\mathbf{q}$ lying on the resonant line ($v_1|q_1| = v_2|q_2| \equiv \omega_{\mathbf{q}}$), both components within the main approximation have the same order of magnitude,

$$\theta_1(x_1, n_2a_2; t) = \theta_0 \cos\left(\frac{1}{2}\phi_{1\mathbf{q}}\omega_{\mathbf{q}}t\right) \times \sin(q_1x_1 + q_2n_2a_2 - \omega_{\mathbf{q}}t),$$

$$\theta_2(n_1a_1, x_2; t) = \theta_0 \sin\left(\frac{1}{2}\phi_{1\mathbf{q}}\omega_{\mathbf{q}}t\right) \times \cos(q_1n_1a_1 + q_2x_2 - \omega_{\mathbf{q}}t).$$

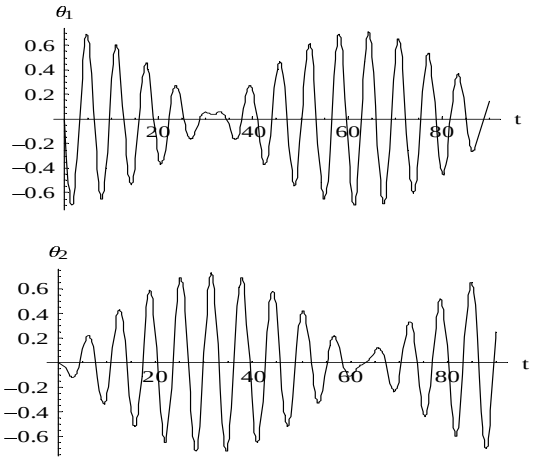

FIG. 13. Periodic energy exchange between arrays (Rabi oscillations)

This corresponds to 2D propagation of a plane wave with wave vector $\mathbf{q}$, *modulated* by a "slow" frequency $\sim \phi\omega$. As a result, beating arises due to periodic energy transfer from one array to another during a long period $T \sim (\phi\omega)^{-1}$ (see Fig.13). These peculiar "Rabi oscillations" may be considered as one of the fingerprints of the physics exposed in QCB systems.

III. TRIPLE QCB

A. Notions and Hamiltonian

Triple quantum bars is $2D$ periodic grid with $m = 3$, formed by three periodically crossed arrays $j = 1, 2, 3$ of $1D$ quantum wires. In fact these arrays are placed on three planes parallel to XY plane and separated by an inter-plane distances d. The upper and the lower arrays correspond to $j = 1, 2$, while the middle array has number $j = 3$. All wires in all arrays are identical. They have the same length L, Fermi velocity v and Luttinger parameter g. The arrays are oriented along the $2D$ unit vectors

$$\mathbf{e}_1 = \left(\frac{1}{2}, \frac{\sqrt{3}}{2}\right), \quad \mathbf{e}_2 = (1, 0), \quad \mathbf{e}_3 = \mathbf{e}_2 - \mathbf{e}_1. \quad (28)$$

The periods of QCB along these directions are equal, $a_j = a$, so we deal with a regular triangular lattice. In what follows we choose $\mathbf{a}_{1,2} = a\mathbf{e}_{1,2}$ as the basic vectors of a superlattice (see Fig.14).

The wires within the j-th array are enumerated with the integers n_j. Define $2D$ coordinates along the n_j-th wire $\mathbf{r}_j$ as $\mathbf{r}_j = x_j\mathbf{e}_j + n_ja\mathbf{e}_3$ for upper and lower arrays ($j = 1, 2$) and $\mathbf{r}_3 = x_3\mathbf{e}_3 + n_3a\mathbf{e}_1$ for the middle array. Here x_j are $1D$ continuous coorinates along the wire. The system of three non-interacting arrays is described by the Hamiltonian

$$H_0 = H_1 + H_2 + H_3, \quad (29)$$

where

$$H_1 = \frac{\hbar v}{2}\sum_{n_1}\int dx_1 \left[g\pi_1^2(x_1\mathbf{e}_1 + n_1a\mathbf{e}_3) + \frac{1}{g}\left(\partial_{x_1}\theta_1(x_1\mathbf{e}_1 + n_1a\mathbf{e}_3)\right)^2\right], \quad (30)$$

$$H_2 = \frac{\hbar v}{2}\sum_{n_2}\int dx_2 \left[g\pi_2^2(x_2\mathbf{e}_2 + n_2a\mathbf{e}_3) + \frac{1}{g}\left(\partial_{x_2}\theta_2(x_2\mathbf{e}_2 + n_2a\mathbf{e}_3)\right)^2\right], \quad (31)$$

$$H_3 = \frac{\hbar v}{2}\sum_{n_3}\int dx_3 \left[g\pi_3^2(x_3\mathbf{e}_3 + n_3a\mathbf{e}_1) + \frac{1}{g}\left(\partial_{x_3}\theta_3(x_3\mathbf{e}_3 + n_3a\mathbf{e}_1)\right)^2\right], \quad (32)$$

and π_j and $\partial_{x_j}\theta_j$ are canonically conjugated fields describing LL within the j-th array.

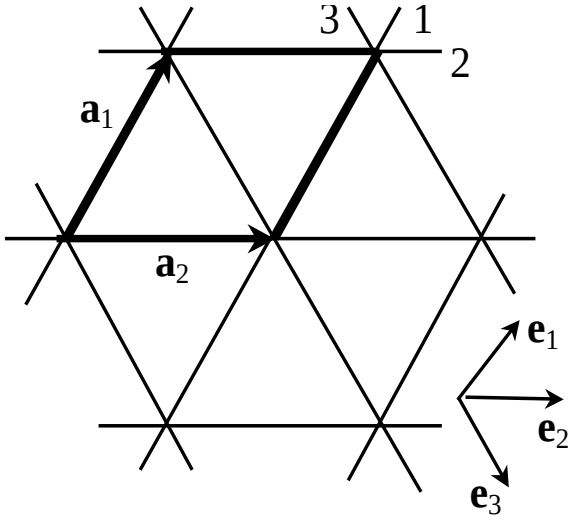

FIG. 14. Triple QCB

Interaction between the excitations in different wires of adjacent arrays j, j' is concentrated near the crossing points with coordinates $n_j\mathbf{a}_j + n_{j'}\mathbf{a}_{j'}$. It is actually Coulomb interaction screened on a distance r_0 along each wire which is described by Hamiltonian

$$H_{int} = H_{13} + H_{23}, \tag{33}$$

where

$$\frac{H_{13}}{V_0} = \sum_{n_1,n_3} \int dx_1 dx_3 \Phi\left(\frac{x_1 - n_3 a}{r_0}\mathbf{e}_1 - \frac{x_3 - n_1 a}{r_0}\mathbf{e}_3\right) \times \partial_{x_1}\theta_1(x_1\mathbf{e}_1 + n_1 a\mathbf{e}_3)\partial_{x_3}\theta_3(n_3 a\mathbf{e}_1 + x_3\mathbf{e}_3), \tag{34}$$

$$\frac{H_{23}}{V_0} = \sum_{n_2,n_3} \int dx_2 dx_3 \Phi\left(\frac{x_2 - n_3 a}{r_0}\mathbf{e}_2 - \frac{x_3 - n_2 a}{r_0}\mathbf{e}_3\right) \times \partial_{x_2}\theta_2(x_2\mathbf{e}_2 + n_2 a\mathbf{e}_3)\partial_{x_3}\theta_3(n_3 a\mathbf{e}_2 + x_3\mathbf{e}_3). \tag{35}$$

Here the effective coupling strength V_0 is defined by Eq.(8), the dimensionless interaction Φ is separable

$$\Phi(\xi_j\mathbf{e}_j + \xi_3\mathbf{e}_3) = \zeta(\xi_j)\zeta(\xi_3), \qquad j = 1, 2, \tag{36}$$

and $\zeta(\xi)$ is dimensionless charge fluctuation in the j-th wire (see Eq. (6)).

Such interaction imposes a superperiodicity on the energy spectrum of initially one dimensional quantum wires, and the eigenstates of this superlattice are characterized by a $2D$ quasimomentum $\mathbf{q} = q_1\mathbf{g}_1 + q_2\mathbf{g}_2 \equiv (q_1, q_2)$. Here $\mathbf{g}_{1,2}$ are the unit vectors of the reciprocal superlattice satisfying the standard orthogonality relations $(\mathbf{e}_i \cdot \mathbf{g}_j) = \delta_{ij}$, $j = 1, 2$. The corresponding basic vectors of the reciprocal superlattice have the form $Q(m_1\mathbf{g}_1 + m_2\mathbf{g}_2$, where $Q = 2\pi/a$ and $m_{1,2}$ are integers. In Fig.15 elementary cell $BIJL$ of the reciprocal lattice is displayed together with the hexagon of the Wigner-Seitz cell that we choose as the BZ of the triple QCB.

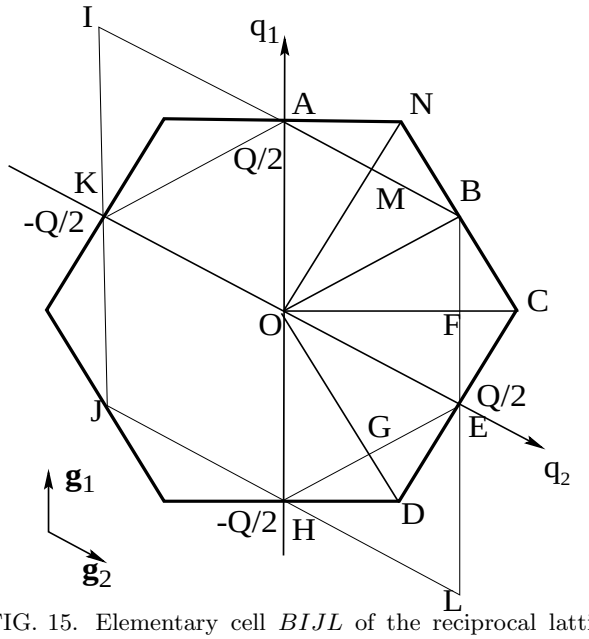

FIG. 15. Elementary cell $BIJL$ of the reciprocal lattice and the BZ hexagon of the triple QCB

To study the energy spectrum and the eigenstates of the total Hamiltonian

$$H = H_0 + H_{int}, \tag{37}$$

we define the Fourier components of the field operators

$$\theta_1(x_1\mathbf{e}_1 + n_1 a\mathbf{e}_3) = (NL)^{-1/2}\sum_{s,\mathbf{q}} \theta_{1s\mathbf{q}} e^{i(q_1 x_1 + q_3 n_1 a)} u_{s,q_1}(x_1), \tag{38}$$

$$\theta_2(x_2\mathbf{e}_2 + n_2 a\mathbf{e}_3) = (NL)^{-1/2}\sum_{s,\mathbf{q}} \theta_{2s\mathbf{q}} e^{i(q_2 x_2 + q_3 n_2 a)} u_{s,q_2}(x_2), \tag{39}$$

$$\theta_3(x_3\mathbf{e}_3 + n_3 a\mathbf{e}_1) = (NL)^{-1/2}\sum_{s,\mathbf{q}} \theta_{3s\mathbf{q}} e^{i(q_3 x_3 + q_1 n_3 a)} u_{s,q_3}(x_3). \tag{40}$$

Here

$$\mathbf{q} = q_1\mathbf{e}_1 + q_2\mathbf{e}_2, \quad q_3 = q_2 - q_1,$$

and $N = L/a$ is the dimensionless length of a wire. In the $\mathbf{q}$ representation, the Hamiltonians H_j (Eqs. (30)-(32)) and H_{j3} (Eqs. (34), (35)) can be written as

$$H_j = \frac{\hbar v g}{2}\sum_{s,\mathbf{q}} \pi^+_{js\mathbf{q}}\pi_{js\mathbf{q}} + \frac{\hbar}{2vg}\sum_{s,\mathbf{q}} \omega_s^2(q_j)\theta^+_{js\mathbf{q}}\theta_{js\mathbf{q}}, \qquad j = 1, 2, 3,$$

$$H_{j3} = \frac{V_0 r_0^2}{2vg}\sum_{s,s',\mathbf{q}} \phi_s(q_3)\phi_{s'}(q_j)\omega_s(q_3)\omega_{s'}(q_j) \times \left[\theta^+_{3s\mathbf{q}}\theta_{js'\mathbf{q}} + h.c.\right], \quad j = 1, 2,$$

where

$$\omega_s(q) = v\left(\left[\frac{s}{2}\right]Q + (-1)^{s-1}|q|\right). \qquad Q = \frac{2\pi}{a}$$

Thus the total Hamiltonian (37) describes a system of coupled harmonic oscillators, and can be diagonalized exactly like in the case of double QCB.

B. Spectrum

Separability of the interaction (36) allows one to derive analytical equations for the spectrum of the total Hamiltonian (37) (see Appendix D). Here we describe the behavior of the spectrum and the states along some specific lines of the reciprocal space.

The high symmetry of the triple QCB leads to a number of lines where interarray or interband resonant interaction occurs: *all* lines in Fig. 15 posess some resonant properties. These lines may be classified as follows:

On the Bragg lines where one of three array wavenumbers q_j is a multiple integer of $Q/2$, there is a strong intraband mixing of modes of the j-th array. In Fig.15, these lines are the boundaries of the elementary cell of the reciprocal lattice $IJLB$, axes q_1 and q_2, lines OB and EH. In particular, along the lines OA ($q_2 = 0$) and OB ($q_3 = 0$) two modes corresponding to 2-d and 3-d bands and to the second (OA) or third (OB) array are mixed. Along the line AB ($q_1 = Q/2$) the same mixing happens between $(1,1)$ and $(1,2)$ modes. Moreover, the resonant mixing of different arrays within the same band occurs along the medians OA, OB, etc.. There are two types of such a resonance. The first of one (e.g. OA line) is the resonance between neighboring arrays ($q_1 = -q_3$) and therefore it is of the main order with respect to interaction. The second one (e.g. OB line) is the resonance between remote arrays ($q_1 = q_2$) and is one order smaller.

The second family consists of resonant lines formed by the BZ hexagon boundaries and diagonals. Thus, the diagonal OC realizes a first order resonance between the first and the third arrays $q_1 = q_3$, and the BZ boundaries HD and AN correspond to the same resonance up to an umklapp process ($q_1 = q_3 - Q$ and $q_1 = q_3 + Q$ respectively). Along the diagonal OD and the BZ boundary NC a second order resonance takes place with resonance conditions $q_2 = -q_1$ and $q_2 = -q_1 + Q$ respectively.

In the reciprocal space of the triple QCB there are four different types of crossing points. Two of them include the bases of BZ medians (e.g. points A, B, E and so on). Here one deals with the four-fold degeneracy of the modes corresponding to the first order resonance between the neighboring arrays (e.g. point A, $\omega_{1,s} = \omega_{3,s'}$, $s, s' = 1, 2$), or to the second order resonance between remote arrays (like point B, $\omega_{1,s} = \omega_{2,s'}$, $s, s' = 1, 2$). One more family consists of crossing points of the BZ diagonals and the lines connecting the bases of its medians (points M, F, G and so on). Here one deals with three types of two-fold degeneracy simultaneously. For example, at the point M two separate pairs of modes corresponding to neighboring arrays $(2,1)$, $(3,1)$, and $(2,2)$, $(3,2)$, are degenerate, as well as two modes corresponding to the first array, $(1,1)$, $(1,2)$. Finally the BZ hexagon vertices form the most interesting group of points where the three-fold degeneracy between modes corresponding to all three arrays takes place. The typical example of such a point is the vertex C where the resonance condition $q_1 = -q_2 + Q = q_3 = Q/3$ is satisfied.

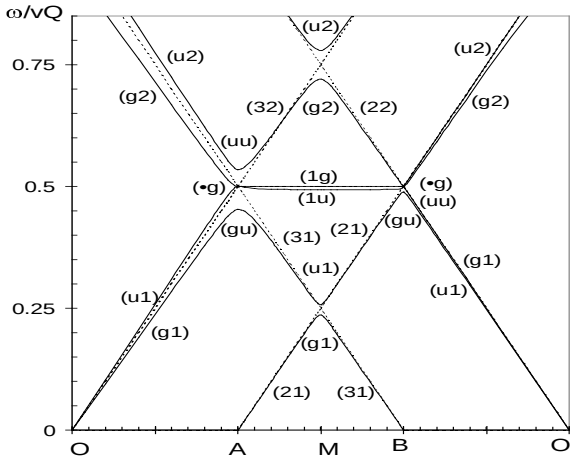

FIG. 16. Dispersion curves at the $OAMBO$ polygon of BZ

Almost all these peculiarities of the triple QCB spectrum can be illustrated in Fig.16 where the dispersion curves along the closed line $OABO$ are displayed. We emphasize once more that in the infrared limit $\omega, \mathbf{q} \to 0$ triple QCB like double QCB preserves the characteristic LL properties of the initial arrays.

C. Observables

The structure of the energy spectrum analyzed above strongly influences optical and transport properties of the triple QCB. As in the case of double QCB (subsection II E), one expects to observe four peaks of the optical absorption near the points A, B, E, H of the four-fold degeneracy. Then, specific features of space correlators like those considered in II E 2 can be observed. But the most pronounced manifestation of a triangular symmetry of the triple QCB are its Rabi oscillations.

Consider the vicinity of the point C of three-fold degeneracy mixing all three arrays. Appropriate initial conditions lead (see Appendix E for details) to the following time dependence of the field operators in the coordinate origin in real space

$$\theta_1(0,0;t) = \theta_0 \sin(\omega_0 t) \cos^2\left(\frac{\sqrt{2\varepsilon}\phi^2}{4}\omega_0 t\right),$$

$$\theta_2(0,0;t) = \theta_0 \cos(\omega_0 t) \sin^2\left(\frac{\sqrt{2\varepsilon}\phi^2}{4}\omega_0 t\right),$$
$$\theta_3(0,0;t) = \theta_0 \sin(\omega_0 t) \cos\left(\frac{\sqrt{2\varepsilon}\phi^2}{2}\omega_0 t\right). \qquad (41)$$

The field operators of all three arrays demonstrate fast oscillations with the resonant frequency ω_0 modulated by a slow frequency. It is the same for the two remote arrays, and doubled for the intermediate array. These beatings are synchronized in a sense that zero intensity on the intermediate array always coincides with the same intensity on one of the remote arrays. At these moments all the energy is concentrated solely within one of the remote arrays. These peculiar Rabi oscillations are displayed in Fig.17.

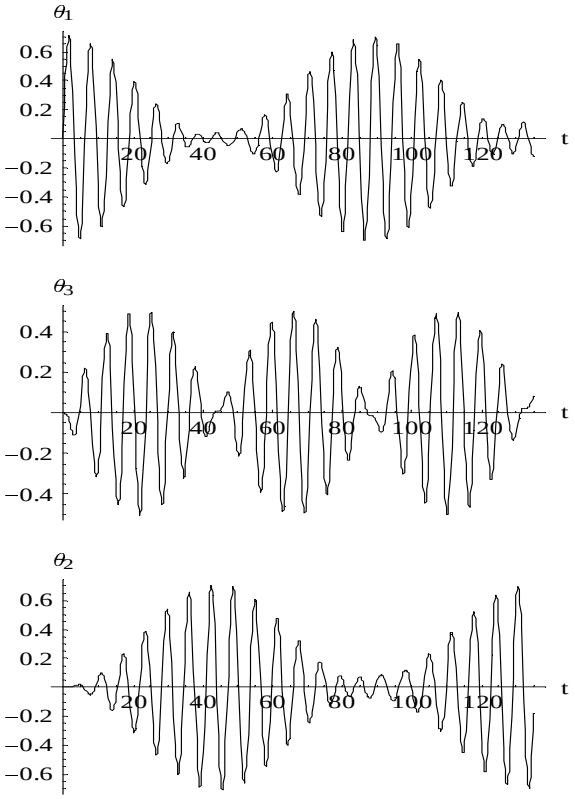

FIG. 17. Periodic energy transfer between three arrays at the triple resonant point C of the BZ

IV. CONCLUSION

We discussed in this paper the kinematics and dynamics of plasmon spectrum in QCB. These nanostructures may be fabricated from single-wall carbon nanotubes[3,24]. On the one hand, QCB is promised to become an important component of future molecular electronics[3,25]. On the other hand, the spectrum of elementary excitations (plasmons) in these grids possesses the features of both 1D and 2D electron liquid. As is shown in Refs. 7,9 and confirmed in the present study, the energy spectrum of QCB preserves the characteristic properties of LL at $|\mathbf{q}|, \omega \to 0$,. At finite $\mathbf{q}, \omega$ the density and momentum waves in double and triple QCB may have either $1D$ or $2D$ character depending on the direction of the wave vector. Due to interarray interaction, unperturbed states, propagating along arrays are always mixed, and transverse components of correlation functions do not vanish. For quasi-momentum lying on the resonant lines of the BZ, such mixing is strong and transverse correlators have the same order of magnitude as the longitudinal ones. Periodic energy transfer betweem arrays ("Rabi oscillations") is predicted.

The crossover from 1D to 2D regime may be experimentally observed. One of the experimental manifestations, i.e. the crossover from isotropic to anisotropic (spatially nonuniform) conductivity was pointed out in Ref. 9. The current may be inserted in QCB at a point on an array j and extracted from another array i at a distance r. Then a temperature dependent length scale $l(T)$ arises, so that for $r \gg l$ the resistance is dominated by small q and therefore, the current is isotropic. In the opposite limit $r < l$ the dependence of the current on the points of injection/extraction may be detected. At $T = 0$ the length l becomes infinite, and current can only be carried along the wires. These effects are in fact manifestations of the LL behavior of the QCB in the infrared limit.

To observe the crossover at finite $\{\omega, \mathbf{q}\}$, one should find a way of exciting the corresponding plasmon modes. Then, scanning the $\omega(q_1, q_2)$ surfaces, one may in principle detect the crossover from quasi 1D to 2D behavior in accordance with the properties of the energy spectra presented in Sections II and III. Plasmons in QCB may be excited either by means of microwave resonators or by means of interaction with surface plasmons. In the latter case one should prepare the grid on a corresponding semiconductor substrate and measure, e.g., the plasmon loss spectra. The theory of these plasmon losses will be presented in a forthcoming publication.

ACKNOWLEDGEMENTS

This research is supported in part by grants from the Israel Science foundations, the DIP German-Israel cooperation program, and the USA-Israel BSF program.

APPENDIX A. EMPTY SUPERCHAIN

Here we construct eigenfunctions, spectrum, and quasi-particle operators for an "empty superchain" -

quantum wire in an infinitely weak periodic potential with period a. Excitations in an initial wire are described as plane waves $L^{-1/2}\exp(ikx)$ with wave number $k = 2\pi n/L$, with integer n, and dispersion law $\omega(k) = v|k|$ (the array number is temporarily omitted). The following orthogonality relations are valid

$$\int_{-L/2}^{L/2} \psi_k^*(x)\psi_{k'}(x)dx = \delta_{k,k'},$$
$$\sum_k \psi_k^*(x)\psi_k(x') = \delta_L(x-x'),$$

where δ_L stands for periodic delta-function

$$\delta_L(x-x') \equiv \sum_n \delta(x-x'-nL).$$

"Empty superchain" is characterized by a space period a and corresponding reciprocal lattice wave number $Q = 2\pi/a$. Each excitation in such a superchain is described by its quasi-wavenumber q and a band number s ($s = 1, 2, \ldots$) that are related to the corresponding wave number k by the following relation,

$$k = q + iQx(-1)^{s-1}\left[\frac{s}{2}\right] \text{ sign } q. \tag{42}$$

The corresponding wave function $\psi_{s,q}(x)$ has the Bloch-type structure,

$$\psi_{s,q}(x) = \frac{1}{\sqrt{L}} e^{iqx} u_{s,q}(x), \tag{43}$$

and satisfies the orthogonality relations

$$\int_{-L/2}^{L/2} \psi_{s,q}^*(x)\psi_{s',q'}(x)dx = \delta_{s,s'}\delta_{Q;q,q'},$$
$$\sum_{s,q} \psi_{s,q}^*(x)\psi_{s,q}(x') = \delta_L(x-x'),$$

where

$$\delta_{Q;q,q'} = \sum_n \delta_{q+nQ,q'}.$$

Within the first BZ, $-Q/2 \le q < Q/2$, Bloch amplitude and dispersion law ω_s have the following form

$$u_{s,q}(x) = \exp\left\{iQx(-1)^{s-1}\left[\frac{s}{2}\right] \text{ sign } q\right\}, \tag{44}$$

$$\omega_s(q) = vQ\left(\left[\frac{s}{2}\right] + (-1)^{s-1}\frac{|q|}{Q}\right). \tag{45}$$

Here square brackets denote an integral part of a number. Taking into account that both Bloch amplitude $u_{s,q}(x)$ and dispersion law $\omega_s(q)$ are periodic functions of q with period Q, one obtaines general equations for the Bloch amplitude

$$u_{s,q}(x) = \sum_{n=-\infty}^{\infty} \frac{\sin\xi_n}{\xi_n} \times \cos[(2s-1)\xi_n]\exp\left(-4i\xi_n\frac{q}{Q}\right),$$
$$4\xi_n = Q(x-na).$$

and dispersion law $\omega_s(q)$

$$(vQ)^{-1}\omega_s(q) = \frac{2s-1}{4} + \sum_{n=1}^{\infty}\frac{2(-1)^s}{\pi^2(2n+1)^2}\cos\frac{2\pi(2n+1)q}{Q}.$$

The relations between quasiparticle operators for a free wire, c_k, for momentum $k \neq nQ/2$ with n integer, and those for an empty superchain, $C_{s,q}$, for quasimomentum q from the first BZ, $-Q/2 < q < Q/2$, look as

$$c_k = C_{s,q}\text{sign}k,$$
$$s = 1 + \left[\frac{2|k|}{Q}\right], \quad q = Q\left(\left\{\frac{k}{Q}+\frac{1}{2}\right\} - \frac{1}{2}\right)$$

$$C_{s,q} = (-1)^\nu c_k,$$
$$k = q + (-1)^\nu Q\left[\frac{s}{2}\right], \qquad \nu = s + 1 + \left[\frac{2q}{Q}\right],$$

where curely brackets denote a fractional part of a number. For obtaining these relations we used the folowing expression

$$\int_{-L/2}^{L/2} \psi_k^*(x)\psi_{s,q}(x)dx = \delta_{s,s(q)}\delta_{Q;q,k}\text{sign}k,$$
$$s(q) = 1 + \left[\frac{2|q|}{Q}\right],$$

for the transition amplitude $\langle k|s,q\rangle$. In case when $k = nQ/2$ with n integer, hybridization of the neighboring bands should be taken into account. This modifies the above relations by the following way

$$c_{nQ/2} = \theta(n)\left[\alpha_n C_{n,q_n} + \beta_n C_{n+1,q_n}\right]$$
$$+\theta(-n)\left[\beta^*_{-n} C_{-n,q_n} - \alpha^*_{-n} C_{-n+1,q_n}\right],$$
$$q_n = Q\left(\left\{\frac{n+1}{2}\right\} - \frac{1}{2}\right);$$

$$C_{s,q_s} = \alpha_s^* c_{sQ/2} + \beta_s c_{-sQ/2},$$
$$C_{s+1,q_s} = \beta_s^* c_{sQ/2} - \alpha_s c_{-sQ/2},$$

where α, β are hybridization coefficients. Corresponding relations between wave functions follow immediately from these formulas.

To write down any of these formulas for a specific array, one should add the array index j to the wave function ψ, Bloch amplitude u, coordinate x, quasimomentum q, and to the periods a and Q of the superchain in real and reciprocal space.

APPENDIX B. DOUBLE QCB SPECTRUM

Here we obtain analytical expressions for dispersion laws and wave functions of QCB. For quasimomenta far from the BZ boundaries, the energy spectrum of the first band can be calculated explicitly. Assuming that $\omega^2 \ll \omega_{js}^2(q_j)$, $s = 2, 3, 4, \ldots$, we omit ω^2 in all terms in the r.h.s. of Eq. (16) except the first one, $s = 1$. As a result the secular equation (17) reads

$$\prod_{j=1}^{2} \left(\frac{\varphi_j^2(q_j)\omega^2}{\omega_j^2(q_j) - \omega^2} + F_j \right) = \frac{1}{\varepsilon}, \tag{46}$$

where

$$\varphi_j^2(q) = \frac{r_j}{a_j}\phi_{j1}^2(q), \qquad \omega_j^2(q) = \omega_{j1}^2(q_j).$$

The solutions of this equation have the form: 2

$$\omega_{\nu 1\mathbf{q}}^2 = \tilde{\omega}_1^2(\mathbf{q}) + \tilde{\omega}_2^2(\mathbf{q}) \pm \sqrt{\left(\tilde{\omega}_1^2(\mathbf{q}) - \tilde{\omega}_2^2(\mathbf{q})\right)^2 + 4\varepsilon\varphi_{\mathbf{q}}^2\omega_1^2(q_1)\omega_2^2(q_2)}. \tag{47}$$

Here

$$\varphi_{\mathbf{q}} = \varphi_1(q_1)\varphi_2(q_2),$$

$\nu = +, -$ is the branch number, $\tilde{\omega}_j(\mathbf{q})$ is determined as

$$\tilde{\omega}_1^2(\mathbf{q}) = \omega_1^2(q_1)\frac{1 - \varepsilon F_1(F_2 - \varphi_2^2(q_2))}{1 - \varepsilon(F_1 - \varphi_1^2(q_1))(F_2 - \varphi_2^2(q_2))} \tag{48}$$

for $j = 1$. Expression for $\tilde{\omega}_2^2(\mathbf{q})$ can be obtained by permutation $1 \leftrightarrow 2$. Parentheses on the r.h.s. of Eq. (48) describe the contributions to F_j from higher bands. Therefore $\tilde{\omega}_j^2(\mathbf{q})$ is the j-th array frequency renormalized by the interaction with higher bands. In principle, contribution of higher bands may turn the interaction to be strong. However for specific case of carbon nanotubes, one stays far from the critical value ε_c (see estimates at the end of subsection II C). Therefore the interaction with higher bands is weak almost in all the BZ except its boundaries.

The resonance line equation modified by interaction with higher bands is

$$\tilde{\omega}_1^2(\mathbf{q}) = \tilde{\omega}_2^2(\mathbf{q}). \tag{49}$$

Out of this line the branch number is in fact the array number and the renormalized frequencies are frequencies of a boson propagating along one of the arrays slightly modified by interactions with the complementary array. In case when $\omega_1(q_1) > \omega_2(q_2)$, one obtains

$$\omega_{+,1\mathbf{q}}^2 \approx \omega_1^2(q_1)\left(1 - \varepsilon F_2\varphi_1^2(q_1)\right). \tag{50}$$

In the opposite case one should replace indices $1 \leftrightarrow 2$, $- \leftrightarrow +$.

Consider the frequency correction in the latter equation in more details. The correction term can be approximately estimated as $\omega_1^2(q_1)S(q_1)$ with

$$S(q_1) = \varepsilon F_2\varphi_1^2(q_1) = \varepsilon\frac{R_0}{a}\phi_{11}^2(q_1)\int d\xi\zeta_2^2(\xi). \tag{51}$$

Due to the short-range character of the interaction, the matrix elements $\phi_{11}(q_1) \sim 1$ vary slowly with the quasimomentum $q_1 \le Q_1$. Therefore, the r.h.s. in Eq.(51) can be roughly estimated as

$$S(q_1) \sim \varepsilon\frac{R_0}{a} = 0.1\frac{R_0}{a} \ll 1. \tag{52}$$

One should also remember that the energy spectrum of nanotube remains one-dimensional only for frequencies smaller than some ω_m. Therefore, an external cutoff arises at $s = ak_m$ where $k_m \sim \omega_m/v$. As a results one gets an estimate

$$S(q_1) \sim \varepsilon\frac{R_0}{a}k_m R_0. \tag{53}$$

Hence, one could hope to gain additional power of the small interaction radius. However, for nanotubes, k_m is of the order of $1/R_0$ (see Refs. 26,23) and both estimates coincide. For quasimomenta close to the BZ center, the coefficient $S(q_1)$ can be calculated exactly. For exponential form of $\zeta(\xi) \propto \exp(-|\xi|)$, one obtains instead of the preliminary estimate (52),

$$S(0) = 0.14\frac{R_0}{a}.$$

Thus, the correction term in Eq.(50) is really small.

The eigenstates of the system are described by renormalized field operators. Within the first band they have the form

$$\tilde{\theta}_{11\mathbf{q}} = \left(1 - \frac{1}{2}\beta_{1\mathbf{q}}\right)(u_{\mathbf{q}}\theta_{11\mathbf{q}} - v_{\mathbf{q}}\theta_{21\mathbf{q}}) - \sum_{s=2}^{\infty}\left(\phi_{1s\mathbf{q}}u_{\mathbf{q}}\theta_{2s\mathbf{q}} + \phi_{2s\mathbf{q}}v_{\mathbf{q}}\theta_{1s\mathbf{q}}\right), \tag{54}$$

$$\tilde{\theta}_{21\mathbf{q}} = \left(1 - \frac{1}{2}\beta_{2\mathbf{q}}\right)(v_{\mathbf{q}}\theta_{11\mathbf{q}} + u_{\mathbf{q}}\theta_{21\mathbf{q}}) - \sum_{s=2}^{\infty}\left(\phi_{1s\mathbf{q}}v_{\mathbf{q}}\theta_{2s\mathbf{q}} + \phi_{2s\mathbf{q}}u_{\mathbf{q}}\theta_{1s\mathbf{q}}\right). \tag{55}$$

Here the coefficients $u_{\mathbf{q}}$ and $v_{\mathbf{q}}$ describe mixing between the modes with different array indices, within the first band,

$$u_{\mathbf{q}} = \sqrt{\frac{\sqrt{\Delta_{\mathbf{q}}^2 + \phi_{1\mathbf{q}}^2} + \Delta_{\mathbf{q}}}{2\sqrt{\Delta_{\mathbf{q}}^2 + \phi_{1\mathbf{q}}^2}}}, \tag{56}$$

$$v_{\mathbf{q}} = \sqrt{\frac{\sqrt{\Delta_{\mathbf{q}}^2 + \phi_{1\mathbf{q}}^2} - \Delta_{\mathbf{q}}}{2\sqrt{\Delta_{\mathbf{q}}^2 + \phi_{1\mathbf{q}}^2}}}, \tag{57}$$

and

$$\Delta_{\mathbf{q}} = \frac{\omega_{21}^2(q_2) - \omega_{11}^2(q_1)}{2},$$
$$\phi_{1\mathbf{q}} = \sqrt{\varepsilon}\varphi_{\mathbf{q}}\omega_{11}(q_1)\omega_{21}(q_2). \tag{58}$$

The parameters $\phi_{1s\mathbf{q}}$, $\phi_{2s\mathbf{q}}$, $s = 2, 3, \ldots$, in Eqs. (54), (55) correspond to inter-band mixing

$$\phi_{1s\mathbf{q}} = \sqrt{\varepsilon}\frac{r_0}{a}\phi_{11}(q_1)\phi_{2s}(q_2)\frac{\omega_{11}(q_1)}{\omega_{2s}(q_2)}, \tag{59}$$

and the coefficients $\beta_{1\mathbf{q}}$, $\beta_{2\mathbf{q}}$, take into account corrections from the higher bands

$$\beta_{1\mathbf{q}} = \sum_{s=2}^{\infty}\left(\phi_{1s\mathbf{q}}^2 u_{\mathbf{q}}^2 + \phi_{2s\mathbf{q}}^2 v_{\mathbf{q}}^2\right). \tag{60}$$

Expressions for $\phi_{2s\mathbf{q}}$ and $\beta_{2\mathbf{q}}$ can be obtained by permutation $1 \leftrightarrow 2$.

Equations (47), (54) and (55) solve the problem of QCB energy spectrum away from the BZ boundaries. However, due to smalness of the interaction, the general expressions (54) and (55) can be simplified. For quasimomenta far from the resonant coupling line, the expressions for the renormalized field operators of the first array look like

$$\tilde{\theta}_{11\mathbf{q}} = \left(1 - \frac{1}{2}\tilde{\beta}_{1\mathbf{q}}\right)\theta_{11\mathbf{q}} + \sum_{s=1}^{\infty}\phi_{1s\mathbf{q}}\theta_{2s\mathbf{q}}, \tag{61}$$

where

$$\phi_{11\mathbf{q}} = \sqrt{\varepsilon}\frac{r_0}{a}\phi_{11}(q_1)\phi_{21}(q_2)\frac{\omega_{11}(q_1)\omega_{21}(q_2)}{\omega_{21}^2(q_2) - \omega_{11}^2(q_1)},$$

and

$$\tilde{\beta}_{1\mathbf{q}} = \sum_{s=1}^{\infty}\phi_{1s\mathbf{q}}^2. \tag{62}$$

The corresponding formulas for the second array are obtained by replacing $1s \to 2s$.

Another simplification is made for modes with quasi–momenta on the resonance line. Consider for simplicity a square QCB (in this case BZ coincides with the elementary cell of the reciprocal lattice, and the resonance line coincides with the BZ diagonal OC in Fig.3) and assume that $\mathbf{q}$ is not too close to the BZ corner C. The initial frequencies of modes belonging to the same band coincide,

$$\omega_{1s\mathbf{q}} = \omega_{2s\mathbf{q}} \equiv \omega_{s\mathbf{q}}. \tag{63}$$

Therefore renormalization strongly mixes the initial variables

$$\tilde{\theta}_{gs\mathbf{q}} = \frac{1}{\sqrt{2}}\left(1 - \frac{1}{2}\beta_{s\mathbf{q}}\right)(\theta_{2s\mathbf{q}} + \theta_{1s\mathbf{q}}) - \frac{1}{\sqrt{2}}\sum_{s'\neq s}(\phi_{s's\mathbf{q}}\theta_{1s'\mathbf{q}} - \phi_{ss'\mathbf{q}}\theta_{2s'\mathbf{q}}),$$

$$\tilde{\theta}_{us\mathbf{q}} = \frac{1}{\sqrt{2}}\left(1 - \frac{1}{2}\beta_{s\mathbf{q}}\right)(\theta_{2s\mathbf{q}} - \theta_{1s\mathbf{q}}) - \frac{1}{\sqrt{2}}\sum_{s'\neq s}(\phi_{s's\mathbf{q}}\theta_{1s'\mathbf{q}} + \phi_{ss'\mathbf{q}}\theta_{2s'\mathbf{q}}),$$

and the corresponding eigenfrequencies are shifted from their bare values

$$\omega_{gs\mathbf{q}}^2 \approx \omega_{s\mathbf{q}}^2\left(1 + \phi_{1s2s\mathbf{q}}\right),$$
$$\omega_{us\mathbf{q}}^2 \approx \omega_{s\mathbf{q}}^2\left(1 - \phi_{1s2s\mathbf{q}}\right).$$

For the first band $s = 1$ these formulas look like

$$\omega_{\pm,1\mathbf{q}}^2 \approx \omega_1^2(q_1)\left(1 \pm \sqrt{\varepsilon}\varphi_{\mathbf{q}}\right). \tag{64}$$

Note that in the resonance case the splitting of the degenerate modes is of the order of $\sqrt{\varepsilon}$ that essentially exceeds the shift of eigenfrequencies in the non-resonant case (50).

The interband mixing becomes significant near the BZ boundaries. Not very close to the crossing points of these boundaries with the resonant lines, this mixing is accounted for by a standard way. As a result we find that the interband hybridization gap for the bosons propagating along the first array can be estimated as

$$\Delta\omega_{12} \sim vQ\varepsilon\frac{r_0}{a}.$$

Similar gaps exist near the boundary of the BZ for each pair of odd and next even energy bands, as well as for each even and next odd band near the lines $q_1 = 0$ or $q_2 = 0$. The energy gap between the s-th and $(s+1)$-th bands is estimated as

$$\Delta\omega_{s,s+1} \sim vQ\varepsilon\frac{r_0}{a}o(s^{-1}).$$

For large enough band number s, the interaction is effectively suppressed, $\phi_{1s2s'} \to 0$, and the gaps vanish.

The spectral behavior in the vicinity of the crossing points of a resonance line and the BZ boundary needs more detailed calculations. Nevertheless it can also be analyzed in a similar way. The results of such an alalysis are discussed in subsubsection II D 1.

APPENDIX C. *AC* CONDUCTIVITY

For interacting wires, where $\phi_{js}(q_j) \neq 0$, the correlator (22) may be easily calculated after diagonalization of the Hamiltonian (9) by means of the transformations (54) and (55). As a result, one has:

$$\left\langle \left[J_{11\mathbf{q}}(t), J^{\dagger}_{11\mathbf{q}}(0) \right] \right\rangle = -2ivg \left(u^2_{\mathbf{q}} \omega_{+,1\mathbf{q}} \sin(\omega_{+,1\mathbf{q}} t) + v^2_{\mathbf{q}} \omega_{-,1\mathbf{q}} \sin(\omega_{-,1\mathbf{q}} t) \right),$$

$$\left\langle \left[J_{11\mathbf{q}}(t), J^{\dagger}_{21\mathbf{q}}(0) \right] \right\rangle = -2ivg u_{\mathbf{q}} v_{\mathbf{q}} \times \left(\omega_{-,1\mathbf{q}} \sin(\omega_{-,1\mathbf{q}} t) - \omega_{+,1\mathbf{q}} \sin(\omega_{+,1\mathbf{q}} t) \right),$$

where $u_{\mathbf{q}}$ and $v_{\mathbf{q}}$ are defined in Eqs.(56), (57). Then, for the optical absorption σ' one obtains

$$\sigma'_{11}(\mathbf{q},\omega) = \pi v g \Big[u^2_{\mathbf{q}} \delta\left(\omega - \tilde{\omega}_{+,1\mathbf{q}}\right) + v^2_{\mathbf{q}} \delta\left(\omega - \tilde{\omega}_{-,1\mathbf{q}}\right) \Big] \quad (65)$$

$$\sigma'_{12}(\mathbf{q},\omega) = \pi v g u_{\mathbf{q}} v_{\mathbf{q}} \Big[\delta\left(\omega - \tilde{\omega}_{-,1\mathbf{q}}\right) - \delta\left(\omega - \tilde{\omega}_{+,1\mathbf{q}}\right) \Big]. \quad (66)$$

For quasimomentum $\mathbf{q}$ away from the resonant coupling line, $u^2_{\mathbf{q}} \approx 1$ and $v^2_{\mathbf{q}} \sim \phi^2_{\mathbf{q}}$ for $\Delta_{\mathbf{q}} > 0$ ($v^2_{\mathbf{q}} \approx 1$ and $u^2_{\mathbf{q}} \sim \phi^2_{\mathbf{q}}$ for $\Delta_{\mathbf{q}} < 0$). Then the longitudinal optical absorption (65) (i.e. the absorption within a given set of wires) has its main peak at the frequency $\omega_{+,1\mathbf{q}} \approx v|q_1|$ for $\Delta_{\mathbf{q}} > 0$ (or $\omega_{-,1\mathbf{q}} \approx v|q_1|$ for $\Delta_{\mathbf{q}} < 0$), corresponding to the first band of the pertinent array, and an additional weak peak at the frequency $\omega_{-,1\mathbf{q}} \approx v|q_2|$, corresponding to the first band of a complementary array. It contains also a set of weak peaks at frequencies $\omega_{2,s\mathbf{q}} \approx [s/2]vQ$ ($s = 2, 3, \ldots$) corresponding to the contribution from higher bands of the complementary array (in Eq.(65) these peaks are omitted). At the same time, a second observable becomes relevant, namely, the transverse optical absorption (66). It is proportional to the (small) interaction strength and has two peaks at frequencies $\omega_{+,1\mathbf{q}}$ and $\omega_{-,1\mathbf{q}}$ in the first bands of both sets of wires.

If the quasimomentum $\mathbf{q}$ belongs to the resonant coupling line $\Delta_{\mathbf{q}} = 0$, then $u^2_{\mathbf{q}} = v^2_{\mathbf{q}} = 1/2$. In this case the longitudinal optical absorption (65) has a split double peak at frequencies $\omega_{+,1\mathbf{q}}$ and $\omega_{-,1\mathbf{q}}$, instead of a single main peak. The transverse optical absorption (66), similarly to the non-resonant case (66), has a split double peak at frequencies $\omega_{+,1\mathbf{q}}$ and $\omega_{-,1\mathbf{q}}$, but its amlitude is now of the order of unity. For $|\mathbf{q}| \to 0$ Eq.(65) reduces to that for an array of noninteracting wires (23), and the transverse optical conductivity (66) vanishes.

The imaginary part of the *ac* conductivity $\sigma''_{jj'}(\mathbf{q},\omega)$ is calculated within the same approach. Its longitudinal component equals

$$\sigma''_{11}(\mathbf{q},\omega) = \frac{2vg}{\omega} \left[\frac{u^2_{\mathbf{q}} \omega^2_{+,1\mathbf{q}}}{\omega^2_{+,1\mathbf{q}} - \omega^2} + \frac{v^2_{\mathbf{q}} \omega^2_{-,1\mathbf{q}}}{\omega^2_{-,1\mathbf{q}} - \omega^2} \right].$$

Beside the standard pole at zero frequency, the imaginary part has poles at the resonance frequencies $\omega_{+,1\mathbf{q}}$, $\omega_{-,1\mathbf{q}}$, and an additional series of high band satellites (omitted here). For quasimomenta far from the resonant lines, only the first pole is well pronounced while amplitude of the second one as well as amplitudes of all other sattelites is small. At the resonant lines, amplitudes of both poles mentioned above are equal. The corresponding expression for $\sigma'_{22}(\mathbf{q},\omega)$ can be obtained by replacement $1 \leftrightarrow 2$.

The transverse component of the imaginary part of the *ac* conductivity has the form:

$$\sigma'_{12}(\mathbf{q},\omega) = \frac{2vg}{\omega} u_{\mathbf{q}} v_{\mathbf{q}} \left[\frac{\omega^2_{-,1\mathbf{q}}}{\omega^2 - \omega^2_{-,1\mathbf{q}}} - \frac{\omega^2_{+,1\mathbf{q}}}{\omega^2 - \omega^2_{+,1\mathbf{q}}} \right].$$

It always contains two poles and vanishes for noninteracting wires. For quasimomenta far from the resonance lines the transverse component is small while at these lines its amplitude is of the order of unity.

APPENDIX D. TRIPLE QCB SPECTRUM

To diagonalize the Hamiltonian(37), we write down equations of motion

$$\left[\omega^2_s(q_j) - \omega^2\right] \theta_{js\mathbf{q}} + \sqrt{\varepsilon} \phi_s(q_j) \omega_s(q_j) \frac{r_0}{a} \sum_{s'} \phi_{s'}(q_3) \omega_{s'}(q_3) \theta_{3s'\mathbf{q}} = 0, \quad (67)$$

$$\left[\omega^2_s(q_3) - \omega^2\right] \theta_{3s\mathbf{q}} + \sqrt{\varepsilon} \phi_s(q_3) \omega_s(q_3) \frac{r_0}{a} \sum_{j,s'} \phi_{s'}(q_j) \omega_{s'}(q_j) \theta_{js'\mathbf{q}} = 0. \quad (68)$$

Here $j = 1, 2$, and ε is defined by Eq.(19). The solutions of the set of equations (67) - (68) have the form:

$$\theta_{js\mathbf{q}} = A_j \frac{\phi_s(q_j)\omega_s(q_j)}{\omega^2_s(q_j) - \omega^2}. \qquad j = 1, 2, 3,$$

Substituting this equation into Eqs.(67) and (68), we have three equations for constants A_j:

$$A_1 + A_3 \sqrt{\varepsilon} F_{q_3}(\omega^2) = 0,$$
$$A_2 + A_3 \sqrt{\varepsilon} F_{q_3}(\omega^2) = 0,$$
$$A_3 + \sum_{j=1,2} A_j \sqrt{\varepsilon} F_{q_j}(\omega^2) = 0,$$

where

$$F_q(\omega^2) = \frac{r_0}{a} \sum_s \frac{\phi^2_s(q) \omega^2_s(q)}{\omega^2_s(q) - \omega^2}. \quad (69)$$

Dispersion relations can be obtained from the solvability condition for this set of equations

$$\varepsilon F_{q_3}(\omega^2)\left(F_{q_1}(\omega^2)+F_{q_2}(\omega^2)\right)=1. \tag{70}$$

The function $F_{q_s}(\omega^2)$ has a set of poles at $\omega^2=\omega_s^2(q)$, $s=1,2,3,\ldots$. For $\omega^2<\omega_s^2(q)$, i.e. within the interval $[0,\omega_1^2(q)]$, $F_{q_s}(\omega^2)$ is positive increasing function. Its minimal value F on the interval is reached at $\omega^2=0$ and does not depend on quasi-momentum q

$$F_q(0)=\frac{r_0}{a}\sum_s \phi_s^2(q)=\int d\xi\zeta_j^2(\xi)\equiv F. \tag{71}$$

If the parameter $\varepsilon\equiv\eta^2$ is smaller than the critical value

$$\varepsilon_c=\frac{1}{2F^2}, \tag{72}$$

then all solutions ω^2 of the characteristic equation are positive. When ε increases, the lowest QCB mode softens and its square frequency vanishes *in whole BZ* at $\varepsilon=\varepsilon_c$. For exponential model $\zeta(\xi)=\exp(-|\xi|)$, one obtains $\varepsilon_c\approx 1$.

APPENDIX E. TRIPLE RABI OSCILLATIONS

The point $C(Q/3,2Q/3)$ of the BZ is the point of threefold degeneracy,

$$q_1=q_3=-q_2+Q=\frac{Q}{3},$$

$$\omega_{11}(Q/3)=\omega_{21}(2Q/3)=\omega_{31}(Q/3)\equiv\omega_0.$$

Equations of motion at this point in the resonance approximation read

$$\left[\frac{d^2}{dt^2}+\omega_0^2\right]\theta_1+\sqrt{\varepsilon}\phi^2\omega_0^2\theta_3=0,$$
$$\left[\frac{d^2}{dt^2}+\omega_0^2\right]\theta_2+\sqrt{\varepsilon}\phi^2\omega_0^2\theta_3=0,$$
$$\left[\frac{d^2}{dt^2}+\omega_0^2\right]\theta_3+\sqrt{\varepsilon}\phi^2\omega_0^2\left(\theta_1+\theta_2\right)=0,$$

where $\theta_j\equiv\theta_{j\mathbf{q}}$. General solution of this system looks as

$$\begin{pmatrix}\theta_1(t)\\ \theta_2(t)\\ \theta_3(t)\end{pmatrix}=\theta_0\begin{pmatrix}1\\ -1\\ 0\end{pmatrix}e^{i\omega_0 t}+$$
$$\theta_+\begin{pmatrix}1\\ 1\\ \sqrt{2}\end{pmatrix}e^{i\omega_+ t}+\theta_-\begin{pmatrix}1\\ 1\\ -\sqrt{2}\end{pmatrix}e^{i\omega_- t},$$

where one of the eigenfrequencies coincides with ω_0, while the two others are

$$\omega_\pm=\sqrt{1\pm\sqrt{2}\phi^2}, \tag{73}$$

and $\theta_{0,\pm}$ are the corresponding amplitudes.

Choosing initial conditions

$$\theta_1(0)=i\theta_0,\qquad \dot\theta_1(0)=\omega_0\theta_0,$$
$$\theta_2(0)=0,\qquad \dot\theta_2(0)=0,$$
$$\theta_3(0)=0,\qquad \dot\theta_3(0)=0,$$

we obtain for the field amplitudes at the coordinate origin

$$\theta_1(0,0;t)=\frac{\theta_0}{4}\left[\frac{\omega_0}{\omega_+}\sin(\omega_+ t)+\frac{\omega_0}{\omega_-}\sin(\omega_- t)\right]$$
$$+\frac{\theta_0}{2}\sin(\omega_0 t),$$
$$\theta_2(0,0;t)=\frac{\theta_0}{4}\left[\frac{\omega_0}{\omega_+}\sin(\omega_+ t)+\frac{\omega_0}{\omega_-}\sin(\omega_- t)\right]$$
$$-\frac{\theta_0}{2}\sin(\omega_0 t),$$
$$\theta_3(0,0;t)=\frac{\theta_0}{2\sqrt{2}}\left[\frac{\omega_0}{\omega_+}\sin(\omega_+ t)-\frac{\omega_0}{\omega_-}\sin(\omega_- t)\right].$$

In the limiting case $\varepsilon\ll 1$ these formulas coincide with Eqs.(41) in subsection **III.C**.

[1] J. Voit, Rep. Prog. Phys. **58**, 977 (1994).
[2] P. W. Anderson, Science **235**, 1196 (1987).
[3] T. Rueckes, K. Kim, E. Joselevich, G. Y. Tseng, C. L. Cheung, and C. M. Lieber, Science **289**, 94 (2000).
[4] H. Dai, Surface Sci, **500**, 218 (2002).
[5] J. von Delft, and H. Schoeller, Ann. der Physik **7**, 225 (1998).
[6] X. G. Wen, Phys. Rev. B **42**, 6623 (1990); H. J. Schultz, Int. J. Mod. Phys. **1/2**. 57 (1991).
[7] V.J. Emery, E. Fradkin, S. A. Kivelson, and T.C. Lubensky, Phys. Rev. Lett. **85**, 2160 (2000).
[8] A. Vishwanath and D. Carpentier, Phys. Rev. Lett. **86**, 676 (2001).
[9] R. Mukhopadhyay, C. L. Kane, and T. C. Lubensky, Phys. Rev. B **63**, 081103(R) (2001); Phys. Rev. B **64**, 045120 (2001).
[10] C. S. Hern, T. C. Lubensky, and J. Toner, Phys. Rev. Lett. **83**, 2745 (1999).
[11] S. L. Sondhi, and K. Yang, Phys. Rev. B **63** 054430 (2001); C. L. Kane, R. Mukhopadhyay, and T. C. Lubensky, Phys. Rev. Lett. **88**, 036401 (2002).
[12] E. Buchstab, A.V.Butenko, and V. V. Pilipenko, Sov. J. Low Temp. Phys. **11**,357 (1985); E. Buchstab, A.V.Butenko, N. Ya. Fogel, V. G. Cherkasova, and R. L. Rosenbaum, Phys.Rev.B **50**, 10063 (1994).
[13] G. Mihaly, I. Kezsmarki, F. Zambroszky, and L. Forro, Phys. Rev. Lett. **84**, 2670 (2000).

[14] Y. Maeno *et al*, Nature **372**, 532 (1994); I. Terasaki, Y. Sasago, and K. Uchinokura, Rev. B **63** RR12685 (1997); S.M. Loureiro *et al*, Rev. B **63** 094109 (2001); I, Tsukada *et al*, cond-mat/0012395 (2000); T. Valla *et al*, Nature, Nature **417**, 627 (2002).
[15] J. E. Avron, A. Raveh, and B. Zur, Rev. Mod.Phys. **60**, 873 (1988).
[16] Y. Avishai, and J. M. Luck, Phys. Rev. B**45**, 1074 (1992).
[17] F. Guinea, and G. Zimanyi, Phys. Rev. B **47**, 501 (1993).
[18] A. H. Castro Neto, and F. Guinea, Phys. Rev. Lett. **80**, 4040 (1998).
[19] I. Kuzmenko, S. Gredeskul, K. Kikoin and Y. Avishai, Fiz. Nizkikh Temp., **28**, 752 (2002).
[20] Y. Luo, C. P. Collier, J.O. Jeppesen, K.A. Nielsen, E. Delonno, G. Ho, J. Perkins, H-R. Tseng, T. Yamamoto, J.F. Stoddardt, J.R. Heath, ChemPhysChem **3**, 519 (2002).
[21] K. Sasaki, cond-mat/0112178.
[22] S.G. Louie in *Carbon Nanotubes*, M.S. Dresselhaus, G. Dresselhaus, Ph. Avouris (Eds.), Topics Appl. Phys. **80**, 113 (2001), Springer, Berlin 2001.
[23] R. Egger, A. Bachtold, M.S. Fuhrer, M. Bockrath, D.H. Cobden, and P.L. McEuen, in *Interacting Electrons in Nanostructures*, p. 125, R. Haug, and H. Schoeller (Eds.), Springer (2001).
[24] M.R. Diehl, S.N. Yaliraki, R.A. Beckman, M. Barahona, and J.R. Heath, Angew. Chem. Int. Ed. **41**, 353 (2002).
[25] G.Y. Tseng and J.C. Ellenbogen, Science **294**, 1293 (2001).
[26] H. Ajiki, and T. Ando, J. Phys. Soc. Jpn. **65**, 505 (1996).